

Unveiling the Quantum Toroidal Dipole in Nanosystems: Quantization, Interaction Energy, and Measurement

Mircea Dolineanu*, Alexandru-Lucian Nastasia † and Dragoş-Victor Anghel‡

January 30, 2024

Abstract

We investigate the physical properties of a charged quantum particle confined to a toroidal surface in the presence of a filiform current along the system's rotational axis. Our analysis reveals that the interaction between the particle and the current induces a non-zero toroidal dipole in the particle's stationary states. We demonstrate that the differences between the toroidal dipole projections for different energy levels can be quantized in units of $\hbar R/(4m_p)$ (where R is the major radius of the torus and m_p is the particle mass), suggesting the existence of toroidal dipole quanta. Furthermore, we find that both the toroidal dipole projection and the energy eigenvalues exhibit periodic behavior with respect to the current intensity, with a period that depends solely on the torus's aspect ratio R/r , where r is the minor radius. This periodicity opens up the possibility of using the current intensity to manipulate and measure the toroidal dipole projection. We also observe abrupt changes in the toroidal dipole projection and energy eigenvalues around integer multiples of the current half-period. These changes provide further evidence for the quantization of the toroidal dipole in such systems. The interaction energy between the particle and the current follows the classical electrodynamics form, suggesting a potential method for measuring and manipulating the toroidal dipole projection along the current axis. The quantization rules we have identified represent hallmarks of the quantum toroidal dipole in nanosystems and could lead to the development of novel devices based on this fundamental property.

Keywords: toroidal dipole operator; quantum observables; nanosystems; metamaterials.

1 Introduction

In 1957, Zeldovich introduced the notion of "anapole" as a multipole moment different from the electric and magnetic ones, which could correspond to the parity non-conserving term introduced by him for describing the β -decay [1],

$$\hat{\mathcal{H}}_\beta \propto \mathbf{S} \cdot \mathbf{J}^{\text{ext}} = \mathbf{S} \cdot (\nabla \times H^{\text{ext}}); \quad (1)$$

in Eq. (1) \mathbf{S} is the spin of the particle and \mathbf{J}^{ext} is the external current corresponding to the external magnetic field H^{ext} . The toroidal dipole was further studied by Dubovik and Cheskov in the framework of classical electrodynamics, who showed that it is related to a third class of multipoles, called toroidal multipoles [2, 3], which are distinct from the usual electric and magnetic multipole families by their symmetry properties under parity and time reversal transformations. A comprehensive review of the multipole expansion in electrodynamics with a clear focus on toroidal moments can be found in the book by Nanz [4]. As the toroidal moments and the anapole have been studied in many contexts, from particle physics to macroscopic physics [5, 6], these concepts were used to describe systems at all scales, like nuclear physics [7], particle physics [8, 9, 10, 11], condensed matter physics [12, 13, 14, 15, 16, 17, 18, 19, 20, 21, 22], and metamaterials [23, 24, 25, 26, 27, 28, 29, 30, 31, 32, 33, 34, 35, 36, 37, 38, 39].

The toroidal dipole, with the expression [13]

$$\mathbf{T} = \frac{1}{10} \int_V [\mathbf{r}(\mathbf{r} \cdot \mathbf{j}) - 2r^2 \mathbf{j}] d^3 \mathbf{r}, \quad (2)$$

*Institutul National de Cercetare-Dezvoltare pentru Fizica si Inginerie Nucleara Horia Hulubei; University of Bucharest, Doctoral School of Physics, mircea.dolineanu@theory.nipne.ro

†Institutul National de Cercetare-Dezvoltare pentru Fizica si Inginerie Nucleara Horia Hulubei; University of Bucharest, Faculty of Physics, alexandru.nastasia@theory.nipne.ro

‡BLTP, JINR, Dubna, Moscow region, 141980, Russia; Institutul National de Cercetare-Dezvoltare pentru Fizica si Inginerie Nucleara Horia Hulubei; *corresponding author* dragos@theory.nipne.ro

where \mathbf{j} is the current density and \mathbf{r} is the position vector, is the lowest order toroidal multipole and the easiest to observe. Toroidal structures of currents, spins, charge distributions or magnetic field distributions, which produce non-zero toroidal dipoles, appear in nuclei, molecules (for example, in benzene, proteins, toroidal carbon cages), biological cells, nanosystems, specially designed metamaterials, etc. (see [5, 14, 24] for examples). Also, toroidal polarizability and transitions could be observed in hydrogen-like atoms [40, 14]. But, despite the obvious differences between toroidal and electrical dipoles, their radiation patterns are identical, which makes them indistinguishable at large distances. This property made many authors question the physical significance of the toroidal dipole and stimulated its study in the near field (see, for example, [36]). The near field properties are important not only to justify the existence of this third class of multipoles, but also because they are responsible for a host of interesting effects, like non-radiating charge-current configurations, nonreciprocal interactions, temperature and refractive index sensing, negative refractive index, cloaking, superlensing, etc. (see [26, 39] and citations therein).

In most of the previously mentioned papers, the toroidal moments are treated in the context of classical electrodynamics. This may be justified for condensed matter, solid state, and metamaterial applications, if the microscopic toroidal structures (the elementary cells in metamaterials) are large enough and quantum effects may be neglected. However, in order to understand what would happen at smaller scales, a quantum approach to toroidal moments is needed, especially, considering that there are possible applications of toroidal moments, for example in dark matter particle models and WISP detection, quantum computing and nanoscale imaging [5, 6]. In this regard, the toroidal dipole operators

$$\hat{T}_i \equiv \frac{1}{10m_p} \sum_{j=1}^3 (x_i x_j - 2r^2 \delta_{ij}) \hat{p}_j, \quad (3)$$

with x_i and \hat{p}_i being the Cartesian position and conjugate momentum operators ($i = 1, 2, 3$), were introduced in [40] in order to study the toroidal polarizability of the hydrogen atom. Later, the mathematical properties of this operator were analyzed in [41], where a first attempt was made at solving the eigenproblem. When the operator was defined on the whole space, it was found to be hypermaximal, and the possibility of it being a quantum observable is questionable. Recently, the operator was particularized for the case of a particle on a torus-shaped nanostructure (see Fig. 1) in the absence of electromagnetic field and a general formalism was established for such systems [42, 43, 44]. The self-adjointness of the operator was proved, therefore the toroidal dipole may be a quantum observable [43]. The eigenvalue problem for this system was also solved, but the results revealed that this operator's eigenstates are outside the Hilbert space of (square integrable) wavefunctions, raising another question regarding to the observability of the toroidal dipole, since the wavefunction cannot collapse on such an eigenvector after an eventual measurement [44].

Once established that the toroidal dipole operator is self-adjoint, we have to understand how this quantum property can be observed or even measured. In the previous studies, no method to measure the toroidal dipole was used or proposed. Instead, some region of the system was studied by some (commercially available, in general) simulation software and the magnetic or current field lines were visually analyzed to identify specific toroidal configurations. This would represent the proof of the presence of toroidal dipoles, which may then be correlated with other specific phenomena, like the cancellation of the electromagnetic radiation at large distances.

Here, we propose a method to identify and measure the toroidal dipole in quantum systems. We start from the interaction Hamiltonian

$$H_I \equiv -\mu_0 q \left[\mathbf{J} + \dot{\mathbf{D}} \right] \cdot \mathbf{T}, \quad (4)$$

which represents the hallmark of the presence of a toroidal dipole in the system, where \mathbf{J} and $\dot{\mathbf{D}}$ are charge and displacement currents, respectively, $\mu_0 = 1.256637 \times 10^{-6} \text{ kg m}/(\text{s}^2 \text{A}^2)$ is the vacuum permeability, and q is the charge of the particle. The interaction (4) of the system with an external current leads to the modification of the energy levels, proportional to the product between the current intensity and the expectation value of the toroidal dipole. Furthermore, if the toroidal dipole expectation values on the Hamiltonian eigenstates are quantized (as we shall see it happens here in most cases), the modification of the energy levels is also quantized, which constitutes an additional verification of the model and of the quantum nature of the toroidal dipole. This method is analog to the detection and measurement of the magnetic moment of a particle, by its interaction with an external magnetic field. In that case also, the energy levels change by amounts proportional to the intensity of the field multiplied to the magnetic moment of the particle. Furthermore, since the projection of the magnetic moment on the field direction is quantized, the splitting of the energy levels is also quantized for a fixed value of the intensity of the field.

The system we study is depicted in Fig. 1. A quantum particle of charge q is confined on a torus, in the presence of a current I which flows along the torus' rotation axis z . We solve the eigenvalues and eigenvectors problem for the

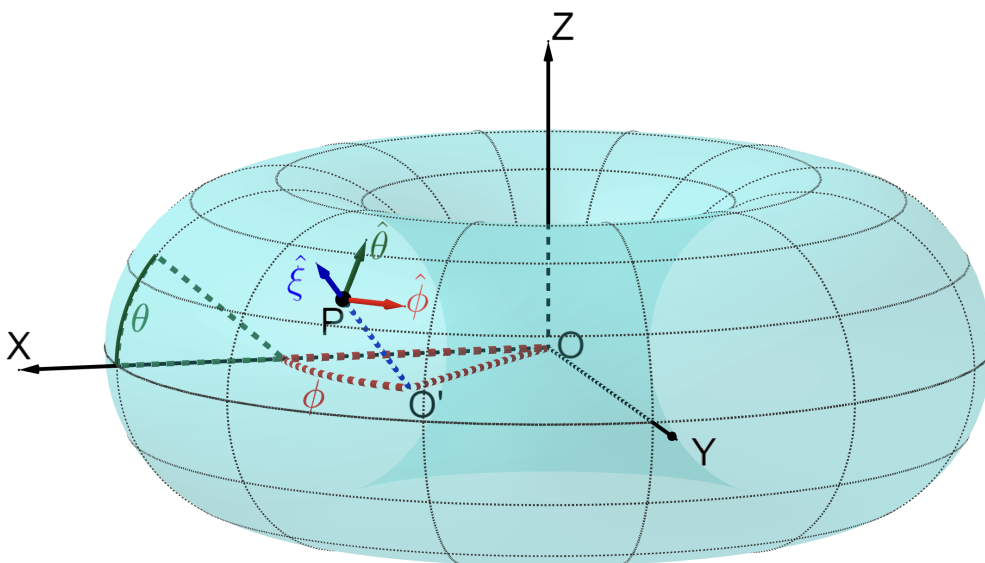


Figure 1: The system of curvilinear coordinates (θ, ϕ, ξ) on a torus made of a thin layer of material. The inner and outer surfaces of the material are two tori with the same major radius R , but minor radii r and $r + \xi_{max}$, respectively, where $r + \xi_{max} < R$ and $\xi_{max} \ll r$ – that is, $\xi = 0$ on the interior surface and $\xi = \xi_{max}$ on the exterior surface; we denote $a \equiv R/r > 1$.

Hamiltonian operator and we calculate the expectation values of the projection \hat{T}_3 (3) of the toroidal dipole operator on the stationary states. We show how the interaction between the current and toroidal dipole induced in the system modify the energy levels, providing in this way a method to measure the toroidal dipole and to show its quantum nature.

The paper is organized as follows. In Section 2 we introduce the formalism and write down the Hamiltonian, together with all the necessary formulas that we shall use in the following sections. In Section 3, we calculate analytically—in the low current limit—the energy levels, the energy eigenstates, and the expectation values of \hat{T}_3 , proving the validity of Eq. (4), together with the quantization of the projection of the toroidal dipole expectation values, which further leads to the quantization of the change of the energy levels. In Section 4 we solve the problem numerically for arbitrary values of I , to find the range of validity of Eq. (4) and of the quantization of the toroidal dipole expectation values. Section 5 is reserved for conclusions and the appendices for some analytical calculations necessary in the main body of the manuscript, but which are not important for the understanding of the physical phenomena presented here.

2 The particle on a torus surface in the presence of an external electromagnetic field

The particle is confined in the region between two tori, as in Fig. 1. Both tori have cylindrical symmetry around the z axis, common origin O (the origin of the Cartesian system of coordinates), the same major radius R , and the minor radii r and $r + \xi_{max}$, where $\xi_{max} \ll r$. We also consider that $r + \xi_{max} < R$, so there is a hole in the middle of the external torus. As in [43], we introduce the coordinates (θ, ϕ, ξ) (ξ replaces here the notation for the coordinate q of [43]), where ϕ is the azimuthal angle, ξ is the coordinate along the minor radius between the inner torus (at $\xi = 0$) and the external torus (at $\xi = \xi_{max}$), whereas θ is the angle formed by the minor radius with the (x, y) plane, as shown in Fig. 1. Then, the Cartesian coordinates (x, y, z) may be written as $x = [R + (r + \xi) \cos \theta] \cos \phi$, $y = [R + (r + \xi) \cos \theta] \sin \phi$, $z = (r + \xi) \sin \theta$, and the corresponding scale factors are $h_\theta = r + \xi$, $h_\phi = R + (r + \xi) \cos \theta$, and $h_\xi = 1$. The determinant of the Jacobian of this transformation is $\det(J) = -(r + \xi) [R + (r + \xi) \cos \theta]$ [43].

2.1 The Hamiltonian

If a spinless particle, of charge q and mass m_p , is in an external electromagnetic field of vector and scalar potentials \mathbf{A} and ϕ , respectively, then its Hamiltonian is

$$\hat{H} = \frac{1}{2m_p} (\hat{\mathbf{p}} - q\mathbf{A})^2 + q\Phi. \quad (5)$$

Writing \hat{H} in the coordinates (θ, ϕ, ξ) and taking into consideration that the system is tightly confined in the ξ direction, then only the coordinates θ and ϕ remain relevant and the Hamiltonian is reduced to the curved 2D surface of the torus [43]:

$$\begin{aligned} \hat{\mathcal{H}}_{elmg}^{2D} &= \hat{\mathcal{H}}_{\text{free}}^{2D} + i \frac{q\hbar}{m_p} \frac{1}{r(R+r\cos\theta)} \left\{ (R+r\cos\theta)A_\theta \frac{\partial}{\partial\theta} + rA_\phi \frac{\partial}{\partial\phi} + \frac{1}{2} \frac{\partial[A_\theta(R+r\cos\theta)]}{\partial\theta} + \frac{r}{2} \frac{\partial(A_\phi)}{\partial\phi} \right\} \\ &\quad + \frac{q^2}{2m_p} (A_\theta^2 + A_\phi^2) + q\Phi, \end{aligned} \quad (6a)$$

where

$$\hat{\mathcal{H}}_{\text{free}}^{2D} = -\frac{\hbar^2 a^2}{2m_p R^2} \left(\frac{\partial^2}{\partial\theta^2} - \frac{\sin\theta}{(a+\cos\theta)} \frac{\partial}{\partial\theta} + \frac{1}{(a+\cos\theta)^2} \frac{\partial^2}{\partial\phi^2} + \frac{a^2}{4(a+\cos\theta)^2} \right) \equiv \frac{\hbar^2}{2m_p R^2} \tilde{\mathcal{H}}_{\text{free}}^{2D} \quad (6b)$$

is the free Hamiltonian, which was analyzed in [43]. In units $\hbar^2/(2m_p R^2)$, $\hat{\mathcal{H}}_{elmg}^{2D}$ becomes

$$\begin{aligned} \hat{\mathcal{H}}_{elmg}^{2D} &= \frac{\hbar^2}{2m_p R^2} \left(\tilde{\mathcal{H}}_{\text{free}}^{2D} + i \frac{a}{a+\cos\theta} \left\{ 2(a+\cos\theta)\tilde{A}_\theta \frac{\partial}{\partial\theta} + 2\tilde{A}_\phi \frac{\partial}{\partial\phi} + \frac{\partial[\tilde{A}_\theta(a+\cos\theta)]}{\partial\theta} + \frac{\partial(\tilde{A}_\phi)}{\partial\phi} \right\} \right. \\ &\quad \left. + (\tilde{A}_\theta^2 + \tilde{A}_\phi^2) + q\tilde{\Phi} \right) \equiv \frac{\hbar^2}{2m_p R^2} \tilde{\mathcal{H}}_{elmg}^{2D}, \end{aligned} \quad (7)$$

where $\tilde{\mathbf{A}} \equiv (qR/\hbar)\mathbf{A}$ and $\tilde{\Phi} \equiv (2m_p R^2/\hbar^2)\Phi$.

Let's assume that through the hole of the torus, along the z axis, passes a thin straight wire of length L , which carries a constant current I (if L is big enough, the circuit may be closed at large distances with additional wires and a current source which would not influence the torus). The vector potential corresponding to this setup is:

$$\mathbf{A} = \left(0, 0, \frac{\mu_0 I}{2\pi} \ln \left(\frac{2L}{\rho} \right) \right), \quad (8)$$

where $\rho = R + r\cos\theta$ is the distance from the z -axis and μ_0 is the vacuum permeability introduced in Eq. (4). Considering that $A_\phi = \mathbf{A} \cdot \hat{\phi}$, $A_\theta = \mathbf{A} \cdot \hat{\theta}$, and $A_\xi = \mathbf{A} \cdot \hat{\xi}$, we can rewrite the vector potential in the (θ, ϕ, ξ) coordinate system:

$$A_\phi = 0, \quad A_\theta = \frac{\mu_0 I}{2\pi} \ln \left(\frac{2L}{\rho} \right) \cos\theta, \quad A_\xi = \frac{\mu_0 I}{2\pi} \ln \left(\frac{2L}{\rho} \right) \sin\theta. \quad (9)$$

Plugging (9) into (7), we obtain

$$\begin{aligned} \tilde{\mathcal{H}}_{elmg}^{(2D)} &= \tilde{\mathcal{H}}_{\text{free}}^{(2D)} + \tilde{\mathcal{H}}_I^{(2D)}, \quad \tilde{\mathcal{H}}_I^{(2D)} \equiv \frac{iI}{I_0} a \log \left(\frac{2a}{a+\cos\theta} \frac{L}{R} \right) \cos\theta \frac{\partial}{\partial\theta} + \frac{iI}{2I_0} \frac{a \sin\theta}{a+\cos\theta} \left[\cos\theta \right. \\ &\quad \left. - (a+2\cos\theta) \log \left(\frac{2a}{a+\cos\theta} \frac{L}{R} \right) \right] + \frac{I^2 \cos^2\theta}{4I_0^2} \log^2 \left(\frac{2a}{a+\cos\theta} \frac{L}{R} \right), \end{aligned} \quad (10)$$

where $I_0 \equiv \pi\hbar/(\mu_0 qR)$ will be our unit of current.

2.2 The momentum operator and the vector basis

Following Refs. [43, 44], we introduce the momentum operators in the coordinates (θ, ϕ, ξ) . The momentum along the ϕ direction is related to the z component of the angular momentum operator (\hat{L}_3), whereas the momentum along the ξ direction is not self-adjoint (because of the boundary conditions), so it is not an observable. The momentum operator along the θ direction is

$$\hat{p}^{(\theta)} \equiv \frac{-i\hbar}{R} a \left\{ \frac{\partial}{\partial \theta} - \frac{\sin \theta}{2(a + \cos \theta)} \right\}. \quad (11)$$

The eigenvectors of $\hat{p}^{(\theta)}$, combined with the eigenvectors of \hat{L}_3 ,

$$\mathcal{F}_{n,m}^{(\Lambda)} \equiv \frac{a}{2\pi R} \frac{e^{i(n\theta+m\phi)}}{\sqrt{a + \cos \theta}} \quad (\text{where } n, m \text{ are integers}), \quad (12)$$

form a basis in the Hilbert space H of wave functions of variables (θ, ϕ) defined on the surface of the torus.

In Ref. [43] we used the basis (12) to numerically diagonalize the operators $\hat{\mathcal{H}}_{\text{free}}^{2D}$ and $\hat{T}_3^{(\theta)}$. In this basis we have the matrix elements

$$\langle \mathcal{F}_{n_1, m_1}^{(\Lambda)} | \tilde{\mathcal{H}}_{\text{free}}^{(2D)} | \mathcal{F}_{n_2, m_2}^{(\Lambda)} \rangle = a^2 \left[\left(n_1^2 - \frac{1}{4} \right) \delta_{n_1 n_2} + \frac{(|\delta n| \sqrt{a^2 - 1} + a) (\sqrt{a^2 - 1} - a)^{|\delta n|}}{(a^2 - 1)^{\frac{3}{2}}} \left(m_1^2 - \frac{1}{4} \right) \right] \delta_{m_1 m_2} \quad (13a)$$

where $\delta n \equiv n_1 - n_2$. From Eq. (13a) we observe that the diagonal elements

$$\langle \mathcal{F}_{n,m}^{(\Lambda)} | \tilde{\mathcal{H}}_{\text{free}}^{(2D)} | \mathcal{F}_{n,m}^{(\Lambda)} \rangle = a^2 \left[\left(n^2 - \frac{1}{4} \right) + \frac{a}{(a^2 - 1)^{\frac{3}{2}}} \left(m^2 - \frac{1}{4} \right) \right] = \langle \mathcal{F}_{-n,m}^{(\Lambda)} | \tilde{\mathcal{H}}_{\text{free}}^{(2D)} | \mathcal{F}_{-n,m}^{(\Lambda)} \rangle \quad (13b)$$

increase linearly with n^2 , whereas the non-diagonal elements ($n_1 \neq n_2$)

$$\langle \mathcal{F}_{n_1, m}^{(\Lambda)} | \hat{\mathcal{H}}_{\text{free}}^{(2D)} | \mathcal{F}_{n_2, m}^{(\Lambda)} \rangle = \frac{a^2 (|\delta n| \sqrt{a^2 - 1} + a) (\sqrt{a^2 - 1} - a)^{|\delta n|}}{(a^2 - 1)^{\frac{3}{2}}} \left(m^2 - \frac{1}{4} \right) \quad (13c)$$

decrease roughly in geometrical progression with $|\delta n|$ because of the factor $(\sqrt{a^2 - 1} - a)^{|\delta n|}$, since $|\sqrt{a^2 - 1} - a| < 1$.

2.2.1 Symmetric and antisymmetric basis vectors

Exploiting the symmetry of the diagonal matrix elements to the change of n into $-n$ (13b) and the fast decrease of non-diagonal elements with $|\delta n|$, we introduce the symmetric (+) and antisymmetric (−) basis vectors

$$\mathcal{F}_{0,m}^{(+)} \equiv \mathcal{F}_{0,m}^{(\Lambda)} \quad \text{and} \quad \mathcal{F}_{n,m}^{(\pm)} \equiv \frac{1}{\sqrt{2}} \left[\mathcal{F}_{n,m}^{(\Lambda)} \pm \mathcal{F}_{-n,m}^{(\Lambda)} \right], \quad (14a)$$

for any $n \in \mathbb{N}^*$ (positive integer), which satisfy the conditions

$$\langle \mathcal{F}_{n_1, m_1}^{(+)} | \mathcal{F}_{n_2, m_2}^{(+)} \rangle = \langle \mathcal{F}_{n_1, m_1}^{(-)} | \mathcal{F}_{n_2, m_2}^{(-)} \rangle = \delta_{n_1, n_2} \delta_{m_1, m_2}, \quad \langle \mathcal{F}_{n_1, m_1}^{(+)} | \mathcal{F}_{n_2, m_2}^{(-)} \rangle = 0. \quad (14b)$$

In the basis (14) we have

$$\begin{aligned} \langle \mathcal{F}_{n,m}^{(\pm)} | \tilde{\mathcal{H}}_{\text{free}}^{(2D)} | \mathcal{F}_{n,m}^{(\pm)} \rangle &= a^2 \left\{ \left[\left(n^2 - \frac{1}{4} \right) + \frac{a}{(a^2 - 1)^{\frac{3}{2}}} \left(m^2 - \frac{1}{4} \right) \right] \pm \frac{(2n\sqrt{a^2 - 1} + a) (\sqrt{a^2 - 1} - a)^{2n}}{(a^2 - 1)^{\frac{3}{2}}} \right. \\ &\quad \left. \times \left(m^2 - \frac{1}{4} \right) \right\}, \end{aligned} \quad (15a)$$

$$\begin{aligned} \langle \mathcal{F}_{n_1, m}^{(\pm)} | \tilde{\mathcal{H}}_{\text{free}}^{(2D)} | \mathcal{F}_{n_2, m}^{(\pm)} \rangle &= a^2 \left\{ \frac{(|n_1 - n_2| \sqrt{a^2 - 1} + a) (\sqrt{a^2 - 1} - a)^{|n_1 - n_2|}}{(a^2 - 1)^{\frac{3}{2}}} \right. \\ &\quad \left. \pm \frac{(|n_1 + n_2| \sqrt{a^2 - 1} + a) (\sqrt{a^2 - 1} - a)^{|n_1 + n_2|}}{(a^2 - 1)^{\frac{3}{2}}} \left(m^2 - \frac{1}{4} \right) \right\}, \quad \text{for } n_1 \neq n_2, \quad \text{and} \end{aligned} \quad (15b)$$

$$0 = \langle \mathcal{F}_{n_1, m}^{(+)} | \tilde{\mathcal{H}}_{\text{free}}^{(2D)} | \mathcal{F}_{n_2, m}^{(-)} \rangle = \langle \mathcal{F}_{n_1, m}^{(-)} | \tilde{\mathcal{H}}_{\text{free}}^{(2D)} | \mathcal{F}_{n_2, m}^{(+)} \rangle. \quad (15c)$$

We observe again the fast increase of the diagonal elements with n , whereas the non-diagonal elements decrease fast with $|n_1 - n_2|$ and $|n_1 + n_2|$. For this reason, the basis (14a) represents a good approximation for the eigenfunctions of $\hat{\mathcal{H}}_{\text{free}}^{(2D)}$ [43] (the higher the energy level n , the better the approximation is).

Equations (15) imply that the Hilbert space H may be split in two: $H \equiv H^{(+)} \oplus H^{(-)}$, where $H^{(+)}$ and $H^{(-)}$ are spanned by the bases $\{\mathcal{F}_{n,m}^{(+)}\}$ and $\{\mathcal{F}_{n,m}^{(-)}\}$, respectively. Then, the eigenfunctions of $\hat{\mathcal{H}}_{\text{free}}^{(2D)}$ belong either to $H^{(+)}$ or to $H^{(-)}$, but they are never a sum of vectors from both spaces.

2.2.2 The matrix elements of the toroidal dipole in the absence of the electromagnetic field

In the absence of the electromagnetic fields, the toroidal dipole operator has the expression (3), which, in the variables (θ, ξ) has the hermitic components [43]

$$\hat{T}_3^{(\theta)} = \frac{\hbar R}{10m_p} \left\{ i \frac{3a \cos(2\theta) + 4(a^2 + 1) \cos \theta + 5a}{2a} \frac{\partial}{\partial \theta} - \tilde{T}_\theta(\theta, \xi) \right\}, \quad (16a)$$

$$\hat{T}_3^{(\xi)} = \frac{\hbar R}{10m_p} \left\{ i \frac{2a^2 + 1 + 3a \cos \theta}{a^2} \sin \theta R \frac{\partial}{\partial \xi} - \tilde{T}_\xi(\theta, \xi) \right\}, \quad (16b)$$

such that $\tilde{T}_\theta(\theta, \xi) = -\tilde{T}_\xi(\theta, \xi)$, so

$$\hat{T}_3 = \hat{T}_3^{(\theta)} + \hat{T}_3^{(\xi)}. \quad (16c)$$

In the limit $\xi_{max} \ll r$, $\tilde{T}_\theta(\theta, \xi)$ and $\tilde{T}_\xi(\theta, \xi)$ are simplified to

$$\tilde{T}_\theta \equiv i \frac{[9a \cos^2 \theta + 2(5a^2 + 2) \cos \theta + a(2a^2 + 3)] \sin \theta}{2a(a + \cos \theta)} = -\tilde{T}_\xi. \quad (16d)$$

The matrix elements of $\hat{T}_3^{(\theta)}$ are [43]

$$\langle \mathcal{F}_{n_1, m_1}^{(\Lambda)} | \hat{T}_3^{(\theta)} | \mathcal{F}_{n_2, m_2}^{(\Lambda)} \rangle = -\frac{\hbar R}{10m_p} \frac{n_1 + n_2}{2a} \left\{ \frac{5a}{2} \delta_{n_1 n_2} + (a^2 + 1) (\delta_{n_1, n_2+1} + \delta_{n_1, n_2-1}) + \frac{3a}{4} (\delta_{n_1, n_2+2} + \delta_{n_1, n_2-2}) \right\} \delta_{m_1 m_2}, \quad (17)$$

which, in the basis (14a), give

$$\langle \mathcal{F}_{n_1, m_1}^{(+)} | \hat{T}_3^{(\theta)} | \mathcal{F}_{n_2, m_2}^{(+)} \rangle = \langle \mathcal{F}_{n_1, m_1}^{(-)} | \hat{T}_3^{(\theta)} | \mathcal{F}_{n_2, m_2}^{(-)} \rangle = 0 \quad (18)$$

for any $n_1 > 0$, $n_2 > 0$, m_1 , and m_2 .

To calculate the expectation values of the whole \hat{T}_3 operator (16c), we first observe that since the eigenstates of the Hamiltonian are stationary states, the probability current in the ξ direction should be zero (no net current flowing in the ξ direction). Taking this into account, plus the conditions (16c) and (16d), the expression for the expectation value of \hat{T}_3 simplifies to

$$\langle \Psi^{(0)} | \hat{T}_3 | \Psi^{(0)} \rangle = \frac{\hbar R}{10m_p} \langle \Psi^{(0)} | \tilde{T}_3^{(j,0)} | \Psi^{(0)} \rangle, \quad \text{where} \quad \tilde{T}_3^{(j,0)} \equiv i \frac{3a \cos(2\theta) + 4(a^2 + 1) \cos \theta + 5a}{2a} \frac{\partial}{\partial \theta} \quad (19)$$

where $\Psi^{(0)}$ is an arbitrary eigenfunction of $\hat{\mathcal{H}}_{\text{free}}^{(2D)}$. In Appendix B we calculate the matrix elements of $\tilde{T}_3^{(j,0)}$ in the basis (12), using the definitions given in Appendix A. Using these matrix elements we obtain a condition similar to (18), namely

$$\langle \mathcal{F}_{n_1, m_1}^{(+)} | \tilde{T}_3^{(j,0)} | \mathcal{F}_{n_2, m_2}^{(+)} \rangle = \langle \mathcal{F}_{n_1, m_1}^{(-)} | \tilde{T}_3^{(j,0)} | \mathcal{F}_{n_2, m_2}^{(-)} \rangle = 0 \quad (20)$$

for any $n_1 > 0$, $n_2 > 0$, m_1 , and m_2 .

Equations (18), (19), and (20) imply that the expectation values of both, $\hat{T}_3^{(\theta)}$ and \hat{T}_3 on the eigenstates of $\hat{\mathcal{H}}_{\text{free}}^{(2D)}$ are zero.

2.2.3 The matrix elements of the interaction Hamiltonian

In the basis (12), the matrix elements of the interaction Hamiltonian (10) are

$$\begin{aligned}
\langle \mathcal{F}_{n_2-n,m}^{(\Lambda)} | \tilde{\mathcal{H}}_I^{2D} | \mathcal{F}_{n_2,m}^{(\Lambda)} \rangle &= \frac{I}{I_0} a \left\{ -\log \left(\frac{2aL}{R} \right) \left[\frac{n_2}{2} (\delta_{n+1} + \delta_{n-1}) + \frac{I_{n+2} - I_{n-2}}{8} \right] - n_2 \left[\frac{\log \frac{2}{a+\sqrt{a^2-1}}}{2} \right. \right. \\
&\times (\delta_{n+1} + \delta_{n-1}) + \left. \frac{I_{n+2} - I_n}{4(n+1)} \Big|_{n+1 \neq 0} + \frac{I_n - I_{n-2}}{4(n-1)} \Big|_{n-1 \neq 0} \right] + \frac{I_{n+2} - I_{n-2}}{8} - \frac{(n+1)I_{n+1}^{(ln^2)} + (n-1)I_{n-1}^{(ln^2)}}{8} \\
&- \frac{a}{4} \left[\log \left(\frac{2aL}{R} \right) (I_{n+1} - I_{n-1}) + nI_n^{(ln^2)} \right] \left. \right\} + \frac{I^2}{16I_0^2} \left\{ \log^2 \left(\frac{2aL}{R} \right) (\delta_{n+2} + 2\delta_n + \delta_{n-2}) \right. \\
&+ \log \left(\frac{2aL}{R} \right) \left[+2 \log \frac{2}{a+\sqrt{a^2-1}} (\delta_{n+2} + 2\delta_n + \delta_{n-2}) + \frac{I_{n+3} - I_{n+1}}{n+2} \Big|_{n+2 \neq 0} + 2 \frac{I_{n+1} - I_{n-1}}{n} \Big|_{n \neq 0} \right. \\
&\left. \left. + \frac{I_{n-1} - I_{n-3}}{n-2} \Big|_{n-2 \neq 0} \right] + \left(I_{n+2}^{(ln^2)} + 2I_n^{(ln^2)} + I_{n-2}^{(ln^2)} \right) \right\} \quad (21)
\end{aligned}$$

where (see Appendix A)

$$I_n(a) \equiv \frac{1}{2\pi} \int_0^{2\pi} \frac{e^{in\theta}}{a + \cos \theta} d\theta = \frac{(-a + \sqrt{a^2 - 1})^{|n|}}{\sqrt{a^2 - 1}}, \quad (22a)$$

$$I_n^{(ln^2)}(a) = \frac{1}{2\pi} \int_0^{2\pi} e^{in\theta} \ln^2(a + \cos \theta) d\theta = \frac{1}{2\pi} \int_0^{2\pi} \cos(n\theta) \ln^2(a + \cos \theta) d\theta. \quad (22b)$$

Using the expression (15) and (21) we write the Hamiltonian matrix in the basis $\{\mathcal{F}_{n,m}^{(\pm)}\}$ (14), which we then diagonalize numerically to obtain the eigenvalues and eigenvectors, as explained in Section 4. Using this basis is especially important in the case $I = 0$, since it preserves the (anti)symmetry of the eigenvectors.

2.3 The toroidal dipole in the presence of electromagnetic fields

In the presence of electromagnetic fields, the definition (3) of the toroidal dipole operator should be changed by taking into consideration the contribution of the fields to the current density operator:

$$\mathbf{j} = \frac{1}{2m_p} (\Psi^* \hat{\mathbf{p}} \Psi - \Psi \hat{\mathbf{p}} \Psi^* - 2q\mathbf{A}|\Psi|^2). \quad (23)$$

With this expression for \mathbf{j} , the components of the toroidal dipole operator change into

$$\hat{T}_i = \frac{1}{10m_p} \sum_{j=1}^3 (x_i x_j - 2r^2 \delta_{ij}) (\hat{p}_j - qA_j). \quad (24)$$

The z component written in toroidal coordinates (θ, ξ) is

$$\hat{T}_3 = -\frac{i\hbar}{10m_p} [z\rho\hat{\mathbf{p}} - (2\rho^2 + z^2)\hat{\mathbf{z}}] \cdot \left[\hat{\boldsymbol{\theta}} \left(\frac{1}{r} \frac{\partial}{\partial \theta} - \frac{iq}{\hbar} A_\theta \right) + \hat{\boldsymbol{\xi}} \left(\frac{\partial}{\partial \xi} - \frac{iq}{\hbar} A_\xi \right) \right], \quad (25)$$

where A_θ and A_ϕ are the components of \mathbf{A} along the $\hat{\boldsymbol{\theta}}$ and $\hat{\boldsymbol{\xi}}$ directions. We split \hat{T}_3 into the hermitic components $\hat{T}_3^{(\theta)}$ and $\hat{T}_3^{(\xi)}$ according to the recipe given in [43] (as we did in Section 2.2.2 for the case without electromagnetic fields), to obtain

$$\hat{T}_3^{(\theta)} = \frac{\hbar R}{10m_p} \left\{ \frac{[z\rho\hat{\mathbf{p}} - (2\rho^2 + z^2)\hat{\mathbf{z}}] \cdot \hat{\boldsymbol{\theta}}}{R^2} \left(-ia \frac{\partial}{\partial \theta} - \frac{qR}{\hbar} A_\theta \right) - \tilde{T}_\theta \right\}, \quad (26)$$

$$\hat{T}_3^{(\xi)} = \frac{\hbar R}{10m_p} \left\{ \frac{[z\rho\hat{\mathbf{p}} - (2\rho^2 + z^2)\hat{\mathbf{z}}] \cdot \hat{\boldsymbol{\xi}}}{R^2} \left(-iR \frac{\partial}{\partial \xi} - \frac{qR}{\hbar} A_\xi \right) - \tilde{T}_\xi \right\}, \quad (27)$$

where \tilde{T}_θ and \tilde{T}_ξ are given in Eqs. (16). Taking into consideration the confinement in the ξ direction, the component of \hat{T}_3 which corresponds to the probability current along ξ —that is, $\partial/\partial\xi - iqA_q/\hbar$ —should be zero on any eigenstate of the Hamiltonian. Taking this into consideration together with (16d), by calculating $\hat{T}_3 \equiv \hat{T}_3^{(\theta)} + \hat{T}_3^{(\xi)}$ we remain only with the term proportional to the probability current along the θ direction:

$$\langle \Psi^{(I)} | \hat{T}_3 | \Psi^{(I)} \rangle \equiv \langle \Psi^{(I)} | \hat{T}_3^{(j)} | \Psi^{(I)} \rangle, \quad (28)$$

where $|\Psi^{(I)}\rangle$ is an eigenstate of the Hamiltonian (10) and

$$\begin{aligned} \hat{T}_3^{(j)} &= -\frac{i\hbar}{10m_p} [z\rho\hat{\rho} - (2\rho^2 + z^2)\hat{z}] \cdot \hat{\theta} \left(\frac{1}{r} \frac{\partial}{\partial\theta} - \frac{iq}{\hbar} A_\theta \right) \equiv \frac{\hbar R}{10m_p} \left(\tilde{T}_3^{(j,0)} + \tilde{T}_3^{(j,I)} \right), \\ \text{with } \tilde{T}_3^{(j,I)} &\equiv \frac{3a \cos(2\theta) + 4(a^2 + 1) \cos\theta + 5a}{2a^2} \tilde{A}_\theta, \end{aligned} \quad (29)$$

whereas A_θ and $\tilde{T}_3^{(j,0)}$ are defined in Eqs. (9) and (19), respectively, and $\tilde{A}_\theta \equiv (qR/\hbar) A_\theta$. The matrix elements of $\tilde{T}_3^{(j,0)}$ and $\tilde{T}_3^{(j,I)}$ are calculated in Appendix B and the final result is

$$\begin{aligned} \langle \mathcal{F}_{n_2-n, m_1}^{(\Lambda)} | \tilde{T}_3^{(j)} | \mathcal{F}_{n_2, m_2}^{(\Lambda)} \rangle &= -\delta_{m_1, m_2} \left(\frac{3}{4} \left(n_2 - \frac{1}{2} \right) \delta_{n_2+2} + \frac{3}{4} \left(n_2 + \frac{1}{2} \right) \delta_{n_2-2} + \frac{1}{4a} [4n_2(a^2 + 1) + a^2 - 2] \delta_{n_2+1} \right. \\ &+ \frac{1}{4a} [4n_2(a^2 + 1) - a^2 + 2] \delta_{n_2-1} + \frac{5n_2}{2} \delta_n - \text{sgn}(n) \frac{(a^2 - 1)}{2} \left(\sqrt{a^2 - 1} - a \right)^{|n|} - \frac{I}{4a^2 I_0} \left\{ \log \left(\frac{2aL}{R} \right) \right. \\ &\times \left[\frac{3a}{4} (\delta_{n+3} + \delta_{n-3}) + (a^2 + 1) (\delta_{n+2} + \delta_{n-2}) + \frac{13a}{4} (\delta_{n+1} + \delta_{n-1}) + 2(a^2 + 1) \delta_n \right] \\ &\left. \left. - \left[\frac{3a}{4} \left(I_{n+3}^{(\text{ln})}(a) + I_{n-3}^{(\text{ln})}(a) \right) + (a^2 + 1) \left(I_{n+2}^{(\text{ln})}(a) + I_{n-2}^{(\text{ln})}(a) \right) + \frac{13a}{4} \left(I_{n+1}^{(\text{ln})}(a) + I_{n-1}^{(\text{ln})}(a) \right) + 2(a^2 + 1) I_n^{(\text{ln})}(a) \right] \right\} \right). \end{aligned} \quad (30)$$

After we diagonalize the Hamiltonian, we use the expression (30) to calculate the expectation values of \hat{T}_3 on the Hamiltonian eigenfunctions, by using the property (28). The results are reported in the next section, together with the diagonalization of the Hamiltonian. In the next sections we shall see that the external electromagnetic fields mix the vector sub-spaces $H^{(+)}$ and $H^{(-)}$ in the Hamiltonian eigenfunctions, so the expectation values of $\hat{T}_3^{(\theta)}$ on these eigenfunctions is not zero for $I \neq 0$.

3 Analytical approximations and the measurement of the toroidal dipole

At large n or a , the diagonal elements of the free particle Hamiltonian in the basis $\{\mathcal{F}_{n,m}^{(+)}, \mathcal{F}_{n,m}^{(-)}\}$ are much bigger than the non-diagonal ones (see Eqs. 15). In such cases, the Hamiltonian eigenfunctions are well approximated by the basis functions [45] and the energy levels are almost double degenerate (15):

$$\begin{aligned} \left| \langle \mathcal{F}_{n,m}^{(+)} | \tilde{\mathcal{H}}_{\text{free}}^{(2D)} | \mathcal{F}_{n,m}^{(+)} \rangle - \langle \mathcal{F}_{n,m}^{(-)} | \tilde{\mathcal{H}}_{\text{free}}^{(2D)} | \mathcal{F}_{n,m}^{(-)} \rangle \right| &= \frac{2(2n\sqrt{a^2 - 1} + a) (\sqrt{a^2 - 1} - a)^{2n}}{(a^2 - 1)^{\frac{3}{2}}} \left| m^2 - \frac{1}{4} \right| \\ \ll \langle \mathcal{F}_{n,m}^{(\pm)} | \tilde{\mathcal{H}}_{\text{free}}^{(2D)} | \mathcal{F}_{n,m}^{(\pm)} \rangle - \langle \mathcal{F}_{n-1,m}^{(\pm)} | \tilde{\mathcal{H}}_{\text{free}}^{(2D)} | \mathcal{F}_{n-1,m}^{(\pm)} \rangle &= (2n - 1) \left[1 \mp \frac{2a^2 (a - \sqrt{a^2 - 1})^{2n-1}}{\sqrt{a^2 - 1}} \right], \end{aligned} \quad (31)$$

since $0 < a - \sqrt{a^2 - 1} < 1$. In such a case, at small values of I , the contribution of $\tilde{\mathcal{H}}_I^{2D}$ to the Hamiltonian may be treated as a perturbation in the 2D space of basis $(\mathcal{F}_{n,m}^{(+)}, \mathcal{F}_{n,m}^{(-)})$. Since a non-zero current I breaks the symmetry of the system, it becomes more convenient to work in the basis $(\mathcal{F}_{n,m}^{(\Lambda)}, \mathcal{F}_{-n,m}^{(\Lambda)})$, which spans the same 2D space. In the new basis, the free Hamiltonian matrix is given by Eqs. (13) and has the symmetric form (69) discussed in Appendix C,

$$A \begin{pmatrix} 1 & \epsilon \\ \epsilon & 1 \end{pmatrix} \mathbf{v} = A\alpha \mathbf{v}, \quad (32a)$$

where

$$A = a^2 \left[\left(n^2 - \frac{1}{4} \right) + \frac{a}{(a^2 - 1)^{\frac{3}{2}}} \left(m^2 - \frac{1}{4} \right) \right] \quad \text{and} \quad \epsilon = \frac{(2n\sqrt{a^2 - 1} + a)(\sqrt{a^2 - 1} - a)^{2n}}{(n^2 - \frac{1}{4})(a^2 - 1)^{\frac{3}{2}} + a(m^2 - \frac{1}{4})}, \quad (32b)$$

with the obvious eigenvalues $\langle \mathcal{F}_{n,m}^{(+)} | \tilde{\mathcal{H}}_{\text{free}}^{(2D)} | \mathcal{F}_{n,m}^{(+)} \rangle$ and $\langle \mathcal{F}_{n,m}^{(-)} | \tilde{\mathcal{H}}_{\text{free}}^{(2D)} | \mathcal{F}_{n,m}^{(-)} \rangle$ and eigenvectors $\mathcal{F}_{n,m}^{(+)}$ and $\mathcal{F}_{n,m}^{(-)}$, respectively.

The matrix elements of the interaction Hamiltonian are

$$\begin{aligned} \langle \mathcal{F}_{nm}^{(\Lambda)} | \tilde{\mathcal{H}}_I^{2D} | \mathcal{F}_{nm}^{(\Lambda)} \rangle &= \frac{an(a - \sqrt{a^2 - 1})I}{I_0} + \frac{I^2}{8I_0^2} \log\left(\frac{2aL}{R}\right) \left\{ \log\left(\frac{2aL}{R}\right) + 2 \log \frac{2}{a + \sqrt{a^2 - 1}} \right. \\ &\quad \left. + \left(a - \sqrt{a^2 - 1} \right)^2 + I_2^{(ln^2)} + I_0^{(ln^2)} \right\}, \end{aligned} \quad (33a)$$

$$\begin{aligned} \langle \mathcal{F}_{-nm}^{(\Lambda)} | \tilde{\mathcal{H}}_I^{2D} | \mathcal{F}_{-nm}^{(\Lambda)} \rangle &= -\frac{an(a - \sqrt{a^2 - 1})I}{I_0} + \frac{I^2}{8I_0^2} \log\left(\frac{2aL}{R}\right) \left\{ \log\left(\frac{2aL}{R}\right) + 2 \log \frac{2}{a + \sqrt{a^2 - 1}} \right. \\ &\quad \left. + \left(a - \sqrt{a^2 - 1} \right)^2 + I_2^{(ln^2)} + I_0^{(ln^2)} \right\}, \end{aligned} \quad (33b)$$

$$\begin{aligned} \langle \mathcal{F}_{-nm}^{(\Lambda)} | \tilde{\mathcal{H}}_I^{2D} | \mathcal{F}_{nm}^{(\Lambda)} \rangle &= \frac{I}{I_0} a \left(\sqrt{a^2 - 1} - a \right)^{2n} \left\{ \log\left(\frac{2aL}{R}\right) \frac{a}{2} + \frac{n}{2} \left(\frac{a - \sqrt{a^2 - 1}}{2n + 1} + \frac{a + \sqrt{a^2 - 1}}{2n - 1} \right) \right. \\ &\quad \left. - \frac{a}{2} - \frac{a}{2} \log\left(\frac{2aL}{R}\right) \right\} + \frac{I^2}{16I_0^2} \log\left(\frac{2aL}{R}\right) \left(\sqrt{a^2 - 1} - a \right)^{2n} \left[\frac{(a - \sqrt{a^2 - 1})^2}{n + 1} + \frac{2}{n} + \frac{(a + \sqrt{a^2 - 1})^2}{n - 1} \right] \\ &\quad - \frac{I}{I_0} a \frac{(2n + 1)I_{2n+1}^{(ln^2)} + (2n - 1)I_{2n-1}^{(ln^2)} + 4naI_{2n}^{(ln^2)}}{8} + \frac{I^2}{16I_0^2} \left(I_{2n+2}^{(ln^2)} + 2I_{2n}^{(ln^2)} + I_{2n-2}^{(ln^2)} \right), \end{aligned} \quad (33c)$$

where we used the expression (22a) for I_n and in the calculation of the non-diagonal elements we assumed $n \geq 2$, so that $2n - 3 \geq 0$ (since we are interested, in general, in large n and a). The matrix elements (33) are added to the matrix elements of the free Hamiltonian and we obtain a matrix of the form (71),

$$A_I \begin{pmatrix} 1 + \delta & \epsilon_I \\ \epsilon_I & 1 - \delta \end{pmatrix} \mathbf{v}_I = A_I \alpha_I \mathbf{v}_I. \quad (34a)$$

where

$$A_I = A + \frac{I^2}{8I_0^2} \log\left(\frac{2aL}{R}\right) \left\{ \log\left(\frac{2aL}{R}\right) - 2 \log(a) + I_2^{(ln^2)} + I_0^{(ln^2)} \right\}, \quad (34b)$$

$$\delta_I = \frac{1}{A_I} \frac{nI}{2I_0}, \quad (34c)$$

$$\epsilon_I = \frac{\epsilon A + \langle \mathcal{F}_{-nm}^{(\Lambda)} | \tilde{\mathcal{H}}_I^{2D} | \mathcal{F}_{nm}^{(\Lambda)} \rangle}{A_I} \quad (34d)$$

Equations (34) have the solutions

$$\alpha_I^{(\pm)} = 1 \pm \sqrt{\epsilon_I^2 + \delta_I^2}, \quad \mathbf{v}_I^{(\pm)} = N_I^{(\pm)} \begin{pmatrix} 1 \\ -\frac{\delta_I}{\epsilon_I} \pm \sqrt{1 + \frac{\delta_I^2}{\epsilon_I^2}} \end{pmatrix}, \quad N_I^{(\pm)} = \frac{1}{\sqrt{2\sqrt{1 + \frac{\delta_I^2}{\epsilon_I^2}} \left(\sqrt{1 + \frac{\delta_I^2}{\epsilon_I^2}} \mp \frac{\delta_I}{\epsilon_I} \right)}}. \quad (35)$$

In Appendix D we calculated analytic approximations for I_n and $I_n^{(ln^2)}$ in the case $a \gg 1$, where we have also

$$a - \sqrt{a^2 - 1} = a \left(1 - \sqrt{1 - 1/a^2} \right) \approx 1/(2a) \ll 1. \quad (36)$$

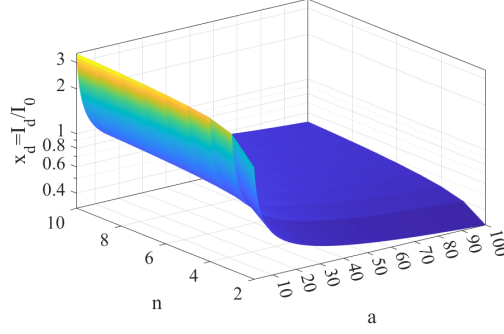


Figure 2: The solution $x_d \equiv I_d/I_0$ of the equation $D(x) = 0$, in the case $m = 0$.

Using the expressions (36) and (77), for $n \geq 2$, Eqs. (33) simplify to

$$\langle \mathcal{F}_{nm}^{(\Lambda)} | \tilde{\mathcal{H}}_I^{2D} | \mathcal{F}_{nm}^{(\Lambda)} \rangle = \frac{nI}{2I_0} \left\{ 1 + \frac{I}{8nI_0} \log\left(\frac{2aL}{R}\right) \log\left(\frac{2L}{R}\right) \right\}, \quad (37a)$$

$$\langle \mathcal{F}_{-nm}^{(\Lambda)} | \tilde{\mathcal{H}}_I^{2D} | \mathcal{F}_{-nm}^{(\Lambda)} \rangle = -\frac{nI}{2I_0} \left\{ 1 - \frac{I}{4nI_0} \log\left(\frac{2aL}{R}\right) \log\left(\frac{2L}{R}\right) \right\}, \quad (37b)$$

$$\begin{aligned} \langle \mathcal{F}_{-nm}^{(\Lambda)} | \tilde{\mathcal{H}}_I^{2D} | \mathcal{F}_{nm}^{(\Lambda)} \rangle &= \frac{I}{I_0} \frac{1}{8a^{2n-2}} \left(\frac{1}{2^{2n-3}(2n-1)} - \left(\sum_{k=1}^{2n-2} \frac{1}{k} \right) - \frac{2(3n-1)}{n(2n-1)} \right. \\ &\quad \left. + \frac{I}{4(n-1)I_0} \left\{ \log\left(\frac{2L}{R}\right) \frac{1}{2^{2n-3}} + \ln a \left[2 + \left(\sum_{k=1}^{2n-3} \frac{1}{k} \right) \right] \right\} \right). \end{aligned} \quad (37c)$$

In the same approximation, the matrix elements of the free Hamiltonian (13) become

$$\langle \mathcal{F}_{n,m}^{(\Lambda)} | \hat{\mathcal{H}}_{\text{free}}^{(2D)} | \mathcal{F}_{n,m}^{(\Lambda)} \rangle = \langle \mathcal{F}_{-n,m}^{(\Lambda)} | \hat{\mathcal{H}}_{\text{free}}^{(2D)} | \mathcal{F}_{-n,m}^{(\Lambda)} \rangle \approx a^2 \left(n^2 - \frac{1}{4} \right) \quad \text{and} \quad \langle \mathcal{F}_{-n,m}^{(\Lambda)} | \hat{\mathcal{H}}_{\text{free}}^{(2D)} | \mathcal{F}_{n,m}^{(\Lambda)} \rangle = \frac{(2n+1)}{(2a)^{2n}} \left(m^2 - \frac{1}{4} \right). \quad (37d)$$

Plugging Eqs. (37) into (34) we obtain

$$A_I = a^2 \left(n^2 - \frac{1}{4} \right) + \frac{I^2}{8I_0^2} \log\left(\frac{2aL}{R}\right) \log\left(\frac{2L}{R}\right), \quad (38a)$$

$$\delta_I = \frac{1}{A_I} \frac{nI}{2I_0} = \frac{nI}{2 \left(n^2 - \frac{1}{4} \right) I_0 a^2} \frac{1}{1 + \frac{I^2}{8 \left(n^2 - \frac{1}{4} \right) I_0^2 a^2} \log\left(\frac{2aL}{R}\right) \log\left(\frac{2L}{R}\right)}, \quad (38b)$$

$$\epsilon_I = \frac{(2n+1) \left(m^2 - \frac{1}{4} \right) (2a)^{-2n} + \langle \mathcal{F}_{-nm}^{(\Lambda)} | \tilde{\mathcal{H}}_I^{2D} | \mathcal{F}_{nm}^{(\Lambda)} \rangle}{A_I}, \quad (38c)$$

$$\frac{\delta_I}{\epsilon_I} = \frac{k_1 I/I_0}{1 + k_2 (I/I_0) + k_3 (I/I_0)^2}, \quad \text{where} \quad (38d)$$

$$k_1 \equiv \frac{n(2a)^{2n}}{2(2n+1) \left(m^2 - \frac{1}{4} \right)}, \quad (38e)$$

$$k_2 \equiv -\frac{2^{2n-3} a^2 \left(\sum_{k=1}^{2n-2} \frac{1}{k} \right) + \frac{2(3n-1)}{n(2n-1)} - \frac{1}{2^{2n-3}(2n-1)}}{\left(m^2 - \frac{1}{4} \right) (2n+1)}, \quad (38f)$$

$$k_3 \equiv \frac{2^{2n-5} a^2 \left[2 + \left(\sum_{k=1}^{2n-3} \frac{1}{k} \right) \right] \ln a + \frac{1}{2^{2n-3}} \log\left(\frac{2L}{R}\right)}{\left(m^2 - \frac{1}{4} \right) (2n+1)(n-1)}, \quad \text{and} \quad n \geq 2. \quad (38g)$$

In the limit $I \rightarrow 0$, $A_I \rightarrow A$, $\delta_I \rightarrow \delta$, $\epsilon_I \rightarrow \epsilon$, and the system (34) transforms into (32), discussed above. Let's analyze now what happens as I increases from zero (because of the symmetry of the system, we shall consider only the case $I \geq 0$). The denominator in the expression (38d) is a second order polynomial that we shall denote by $D(x) \equiv 1 + k_2x + k_3x^2$, with $x \equiv I/I_0$. If $m = 0$, then $k_2 > 0$ whereas $k_1, k_3 < 0$. Calculating the derivative $D'(x) = k_2 + 2k_3x$, we observe that both, $D(0)$ and $D'(0)$ are positive at $x = 0$. Since $\lim_{x \rightarrow \infty} D(x) = -\infty$, this implies that for $m = 0$, $D(x)$ has one and only one solution at $x > 0$, namely

$$x_d \equiv \frac{I_d}{I_0} = \frac{-k_2 - \sqrt{k_2^2 - 4k_3}}{2k_3}. \quad (39)$$

(see Fig. 2). Calculating

$$\frac{d(\delta_I/\epsilon_I)}{d(I/I_0)} = \frac{k_1 [1 - k_3(I/I_0)^2]}{[k_3(I/I_0)^2 + k_2I/I_0 + 1]^2}, \quad (40)$$

we observe that for $m = 0$, $d(\delta_I/\epsilon_I)/d(I/I_0) < 0$ for any I . Since $\delta_I/\epsilon_I|_{I=0} < 0$, Eq. (40) implies that $\delta_I/\epsilon_I|_{I < I_d} < 0$ and $\delta_I/\epsilon_I|_{I > I_d} > 0$, whereas $\delta_I/\epsilon_I|_{I=I_d}$ is divergent. In Fig. 3 we plot the δ_I/ϵ_I for $n = 2, 3, 5$. We see that in the vicinity of $I = 0$, δ_I/ϵ_I increases very fast with I , especially when a or n are big.

For $m \neq 0$, $k_1, k_3 > 0$ and $k_2 < 0$. The function δ_I/ϵ_I is positive at $I = 0$, whereas its derivative (40), also positive at $I = 0$, is equal to zero at

$$\frac{I_{\max}}{I_0} = \frac{1}{\sqrt{k_3}}, \quad (41)$$

where δ_I/ϵ_I reaches its local maximum

$$\left(\frac{\delta_I}{\epsilon_I}\right)_{\max} = \frac{k_1}{k_2 + 2\sqrt{k_3}}. \quad (42)$$

The ratio I_{\max}/I_0 is plotted in Fig. 4 and in Fig. 5 we plot δ_I/ϵ_I for $m = 1$ and $n = 2, 3, 5$.

From Eqs. (38) and Figs. (3) and (5) we observe that if $n \geq 2$ and $a \gg 1$ (in practice, $a > 2$ is enough in most cases) the ratio δ_I/ϵ_I increases very fast with I in the vicinity of $I = 0$. From Eq. (40) we find the slope

$$\lim_{I \rightarrow 0} \left[\frac{d(\delta_I/\epsilon_I)}{d(I/I_0)} \right] = k_1, \quad (43)$$

plotted in Fig. 6. Therefore, we may find a range for I , such that $I/I_0 \ll 1 \ll k_1I/I_0$ and $\delta_I/\epsilon_I \gg 1$. In such a case, as we showed in the end of Appendix C, the eigenvectors of the Hamiltonian converge to $(\mathcal{F}_{n,m}^{(\Lambda)}, \mathcal{F}_{-n,m}^{(\Lambda)})$, with the corresponding eigenvalues

$$\tilde{E}_n^{(\pm)} = \langle \mathcal{F}_{\pm n,m}^{(\Lambda)} | \tilde{\mathcal{H}}_{\text{elmg}}^{2D} | \mathcal{F}_{\pm n,m}^{(\Lambda)} \rangle = A_I \alpha_I^{(\pm)} = A_I (1 \pm \delta_I) = A \pm \frac{nI}{2I_0}. \quad (44a)$$

We observe, therefore, a splitting of the quasi-degenerate energy levels by

$$\Delta \tilde{E}_n^{(I)} = n \frac{I}{I_0}. \quad (44b)$$

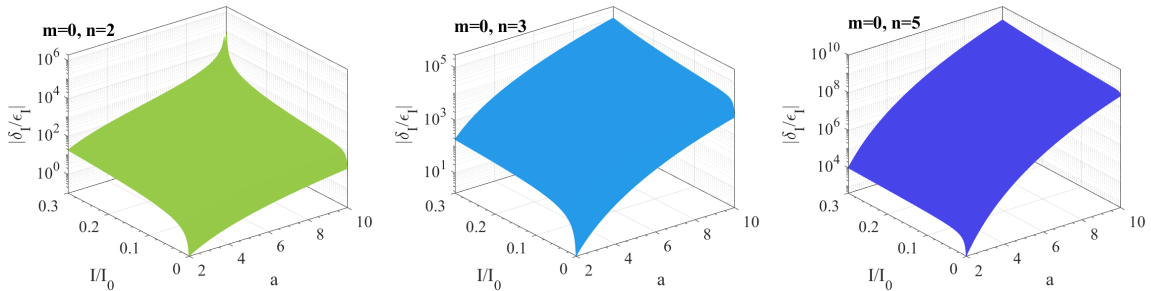


Figure 3: The ratio $|\delta_I/\epsilon_I|$ in the case $m = 0$ and $n = 2, 3, 5$, as indicated in each plot (for $m = 0$, $\delta_I/\epsilon_I < 0$ for small values of I/I_0).

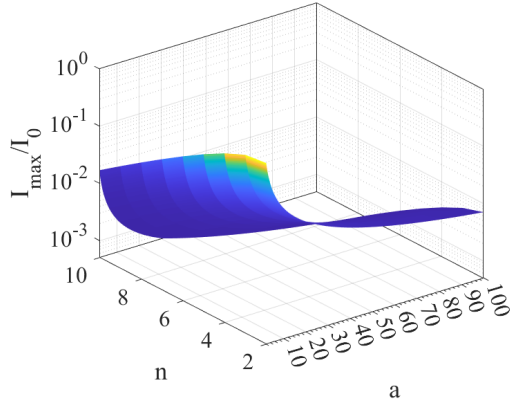


Figure 4: The ratio I/I_0 at which δ_I/ϵ_I reaches its maximum for $m \neq 0$, $n \geq 2$, and $a \geq 2$.

Further, the expectation values of \tilde{T}_3 on the Hamiltonian eigenstates (see Eq. 30) have very simple values,

$$\langle \tilde{T}_3 \rangle_n = \langle \mathcal{F}_{n,m}^{(\Lambda)} | \tilde{T}_3 | \mathcal{F}_{n,m}^{(\Lambda)} \rangle = -\frac{5n}{2} = -\langle \mathcal{F}_{-n,m}^{(\Lambda)} | \tilde{T}_3 | \mathcal{F}_{-n,m}^{(\Lambda)} \rangle \equiv -nt_3^{(0)}. \quad (45)$$

Notice that $t_3^{(0)} = 5/2$ is different from the quanta t_3 of the eigenvalues of the operator $\hat{T}_3^{(\theta)}$ obtain in Ref. [44]. Combining Eqs. (44) and (45) we obtain

$$\Delta \tilde{E}_n^{(I)} = -\frac{2}{5} \frac{I}{I_0} \langle \tilde{T}_3 \rangle_n. \quad (46)$$

Including the dimensional scales for energy (7) and toroidal dipole (16), we obtain the linear relation between the energy deviation and toroidal dipole

$$\frac{\Delta E_n^{(I)}}{2} \equiv \frac{\hbar^2}{2m_p R^2} \frac{\Delta \tilde{E}_n^{(I)}}{2} = -\mu_0 q \frac{I}{\pi R^2} \langle \tilde{T}_3 \rangle_n, \quad (47)$$

which is identical to (4), if we make the natural identification for the current density, $j \equiv I/(\pi R^2)$.

Equation (47) gives us a direct method to observe the toroidal dipole and to measure its expectation values. In this way one may observe also the quantization (45), as a proof of the quantum nature of T_3 .

4 Numerical study of stationary states and toroidal moment values

For numerical computations we use $L = 2000$ nm and $R = 250$ nm, whereas the filiform current I (flowing along the z axis) and the torus' minor radius r , characterized by the parameter $a \equiv R/r$, are varying (see Fig. 1).

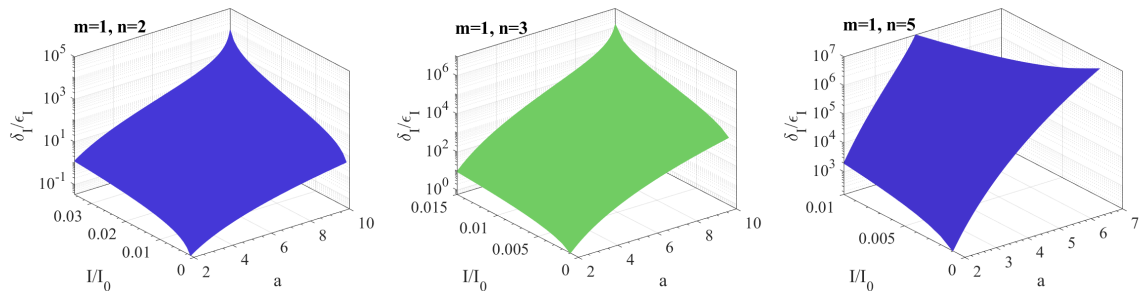


Figure 5: The ratio δ_I/ϵ_I for $m = 1$ and $n = 2, 3, 5$, as indicated in each plot.

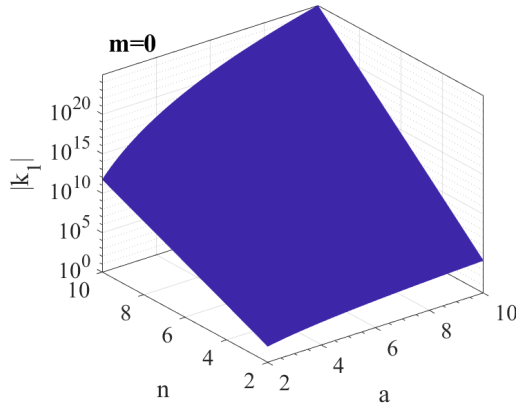


Figure 6: The absolute value of the slope $d(\delta_I/\epsilon_I)/d(I/I_0)$ at $I = 0$ and $m = 0$.

The Hamiltonian of the system is given by Eqs (10) and (6b). Similarly to the procedure detailed in [43], we numerically computed the matrix elements $\langle \mathcal{F}_{n_1, m_1}^{(\pm)} | \tilde{\mathcal{H}}^{(2D)} | \mathcal{F}_{n_2, m_2}^{(\pm)} \rangle$ using the expressions (15) and (21), and we performed numerical diagonalization. The energy levels as functions of I are shown in Fig. 7 for different values of a and m . In connection to these, we calculated the expectation values of \tilde{T}_3 on the Hamiltonian eigenstates (using Eq. 30), which we plot in Figs. 8 and 9. We index the energy levels by $\eta = 0, 1, 2, \dots$, starting from the ground state and going up in energy. Therefore, the Hamiltonian eigenvalues and eigenstates will be denoted by $E_\eta(I)$ and $|\Psi_\eta(I)\rangle$, such that $E_\eta(I) \leq E_{\eta'}(I)$ if $\eta < \eta'$. For the expectation values of \tilde{T}_3 we shall use the simpler notation $\langle \tilde{T}_3 \rangle_\eta(I) \equiv \langle \Psi_\eta(I) | \tilde{T}_3 | \Psi_\eta(I) \rangle$. To keep the notations simple, the dependence of $|\Psi_\eta(I)\rangle$, $E_\eta(I)$, and $\langle \tilde{T}_3 \rangle_\eta(I)$ on a and m will be considered implicit. Even more, sometimes we may consider implicit also dependence of these quantities on I . Comparing this notation with the one used in Eqs. (44), we observe that, if the approximations of Section 3 apply, then

$$E_{\eta=2n-1} \approx E_n^{(-)} \quad \text{and} \quad E_{\eta=2n} \approx E_n^{(+)}.$$
 (48a)

In Eqs. (44) and (48b) we have $n > 0$, since $E_n^{(+)}$ and $E_n^{(-)}$ refer to n and $-n$, respectively. To avoid confusion, from now on we shall use the correspondence

$$\eta \equiv \begin{cases} 2n, & \text{if } n > 0, \\ -2n - 1, & \text{if } n < 0. \end{cases}$$
 (48b)

At $I = 0$, the energy levels (see Fig. 7) are the same as the ones calculated in [43] and the expectation values of \tilde{T}_3 are zero, as proved in Section 2.2.2 (Fig. 9). In the presence of the external current, the energy levels change and the energy eigenstates acquire non-zero toroidal dipole. The cause of the energy levels change is the interaction between the toroidal dipoles and the current—analogously to the modification of the energy levels of a particle with nonzero magnetic moment, in the presence of an external magnetic field. Both, $E_\eta(I)$ and $\langle \tilde{T}_3 \rangle_\eta(I)$ show a periodic patterns which depend only on a (and are independent of η and m).

To understand this better, let's look at Fig. 9. If a or η are sufficiently large, $\langle \tilde{T}_3 \rangle_\eta(I)$ varies rapidly with I/I_0 , approaching the value $-5n/2$ (48b), in accordance with the analytical calculations of Section 3. It is not necessary to give here a precise definition for when “ a or η are sufficiently large” and we shall give it only a qualitative significance. For example, we may roughly say that this condition is satisfied for the levels 7 to 10 of panel (a), levels 5 to 10 of panels (d) and (e), levels 7 to 10 of panel (f), levels 3 to 10 of panel (g), and levels 5 to 10 of panels (h) and (i).

On a larger interval of currents (see Fig. 8), if a or η are sufficiently large, we observe that $\langle \tilde{T}_3 \rangle_\eta(I)$ decreases linearly with I , having abrupt changes of sign at regular intervals lI_s , where l is an integer and I_s depends on a , but not on η or m . In each interval of linear variation included between the limits lI_s and $(l+1)I_s$, the slope $d\langle \tilde{T}_3 \rangle_\eta(I)/d(I/I_0) = -(5/4)(I_0/I_s)$, is the same for any m , l , a , and η . Therefore, the decrease of the linear approximation of $\langle \tilde{T}_3 \rangle_\eta(I)$ on any interval $(lI_s, (l+1)I_s)$ takes the universal value of $5/4$, independent of current, angular momentum, shape of the torus or energy level, as long as a or η are sufficiently large. Moreover, differences

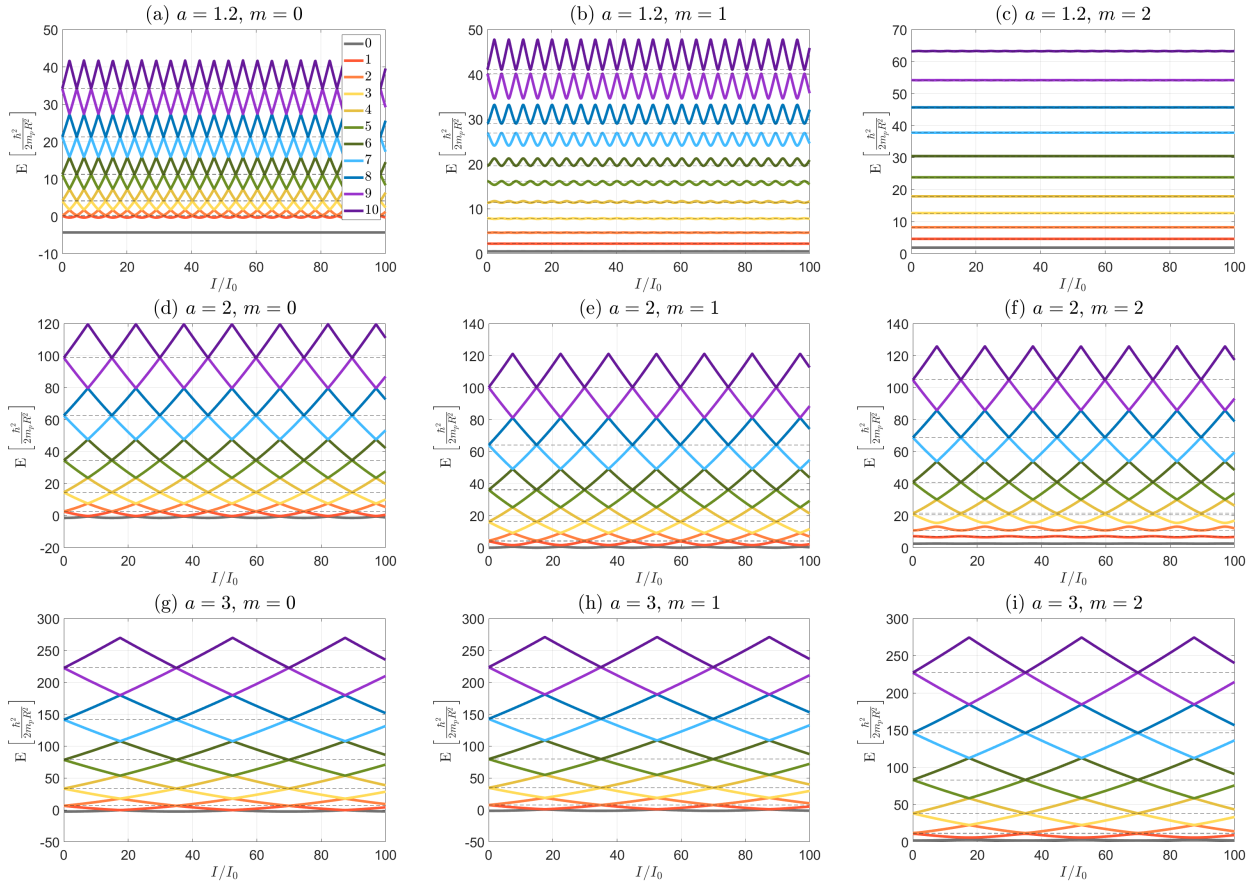


Figure 7: The energies (in dimensionless units) of the first eleven Hamiltonian eigenstates as functions of I (in I_0 units) for $a = 1.2, 2, 3$ and $m = 0, 1, 2$, as indicated in each plot. The legend, shown in (a), is the same in every plot: 0 = ground state, 1 = first excited state, and so on.

between expectation values take also universal forms

$$\langle \tilde{T}_3 \rangle_\eta(I) - \langle \tilde{T}_3 \rangle_{\eta-1}(I) = \frac{(-1)^{\eta-1} 5}{2} \eta \quad \text{and} \quad \langle \tilde{T}_3 \rangle_\eta(I) - \langle \tilde{T}_3 \rangle_{\eta-2}(I) = \frac{(-1)^{\eta-1} 5}{2}, \quad (49)$$

which are valid for any current I , torus shape a , angular momentum m , or energy level η , if a and η are large enough and the current is in the region where $\langle \tilde{T}_3 \rangle_\eta(I)$ varies linearly, as seen in Fig. 8. For all values of a and m (not only when a and η are sufficiently large), the functions $\langle \tilde{T}_3 \rangle_\eta(I)$ are periodic, of period $2I_s$.

In Fig. 7 we plot the energy levels $E_\eta(I)$ as functions of I/I_0 for a few values of a and m . We clearly see same periodicity, of period $2I_s$, as in Fig. 7. For the levels where a and η are sufficiently large, the variation of $E_\eta(I)$ is proportional to $I \langle \tilde{T}_3 \rangle_\eta(I)$, as we proved in Section 3 (Eq. 47) and we can see in Fig. 10. The numerical calculations show that the validity of the proportionality relation (47) extends over a larger interval of currents than that on which the approximations of Section 3 are valid. At $I = lI_s$ ($l > 0$), the functions $E_\eta(I)$ are continuous, but their derivatives change abruptly.

In Fig. 11 we plot the first coefficients of the expansion of the energy eigenstates in the basis formed by the momentum eigenstates $\{\mathcal{F}_{n,m}^{(\Lambda)}\}$. In all the plots, at $I = 0$ we obtain again the coefficients from Ref. [43], but, as I increases, the wavefunctions significantly change.

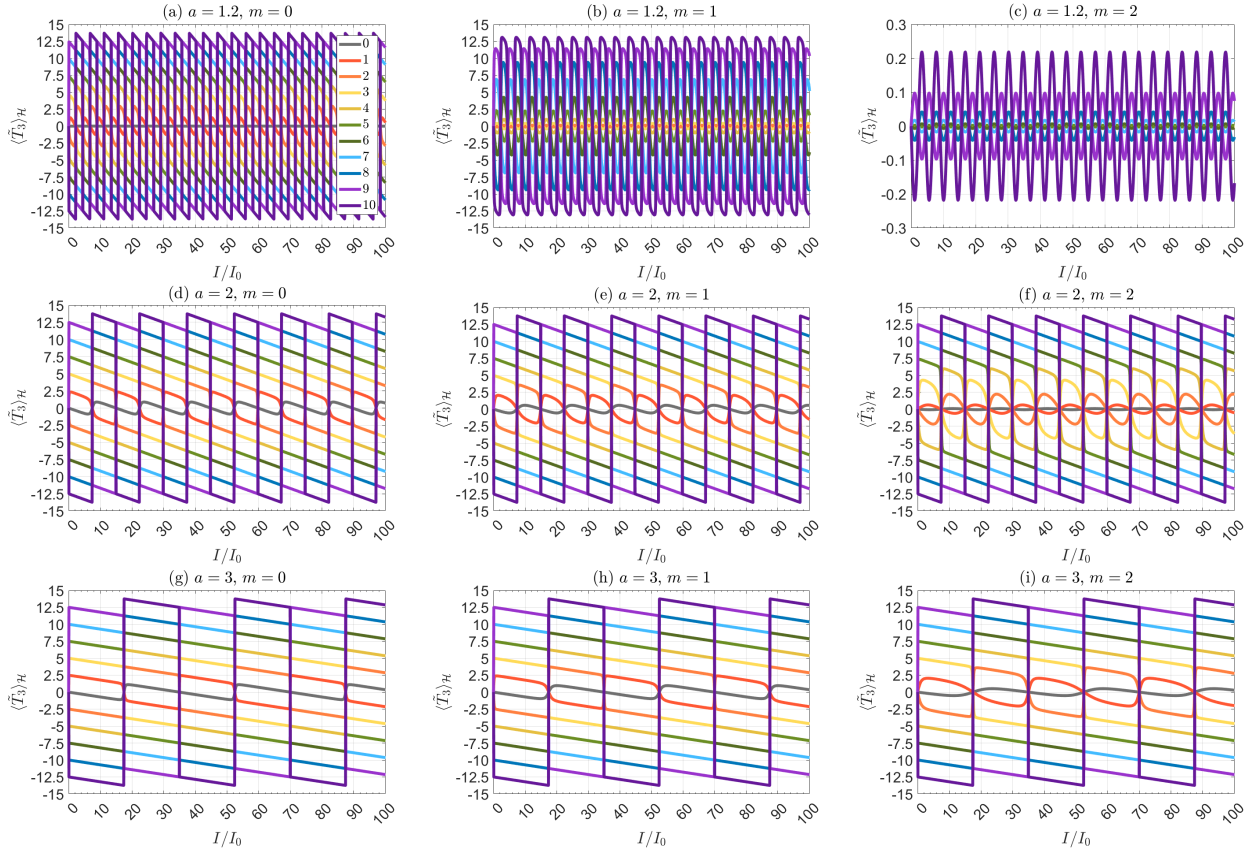


Figure 8: The expectation values of \tilde{T}_3 on the Hamiltonian eigenstates vs. I (in I_0 units) for $a = 1.2, 2, 3$ and $m = 0, 1, 2$, as indicated in each plot. The legend, shown only once, is the same in every plot: 0 = ground state, 1 = first excited state, 2 = second excited state, ...

5 Conclusions

In this work, we studied the quantum properties of a particle on a torus in the presence of a filiform current flowing along the rotational axis of the system. We observed the quantization of the energy levels and their dependence on the current intensity and we calculated the expectation values of the projection of the toroidal dipole operator on the rotation axis in the stationary states. We showed that the expectation values are zero if the current is zero, but they become non-zero in the presence of non-zero current, providing a method to observe and measure the quantum toroidal dipole.

Our analytical and numerical calculations revealed several important features of the system. First, we found that the energy levels and the expectation values of the toroidal dipoles are periodic functions of the current intensity, with period $2I_s$, where I_s depends only on the aspect ratio of the torus. Second, we observed that the derivative of the energy with respect to the current intensity, as well as the expectation values of the toroidal dipole exhibit sharp changes of sign at integer multiples of I_s . Third, we found that the toroidal dipole moment decreases linearly with current outside of these narrow regions, with a universal change in its scaled, dimensionless value equal to $-5/4$ over half-period. Fourth, we showed that the differences between the toroidal dipole moments of consecutive and second consecutive energy levels exhibit universal forms. Fifth (and maybe the most significant), in general, the changes, due to transitions between energy levels, of the expectation values of the toroidal dipole are quantized, the scaled, dimensionless value of the quanta being $5/2$.

Our results provide a theoretical framework for understanding the interaction between a particle with a toroidal dipole moment and an external current. They also pave the way for the experimental observation and measurement of toroidal dipoles in quantum systems.

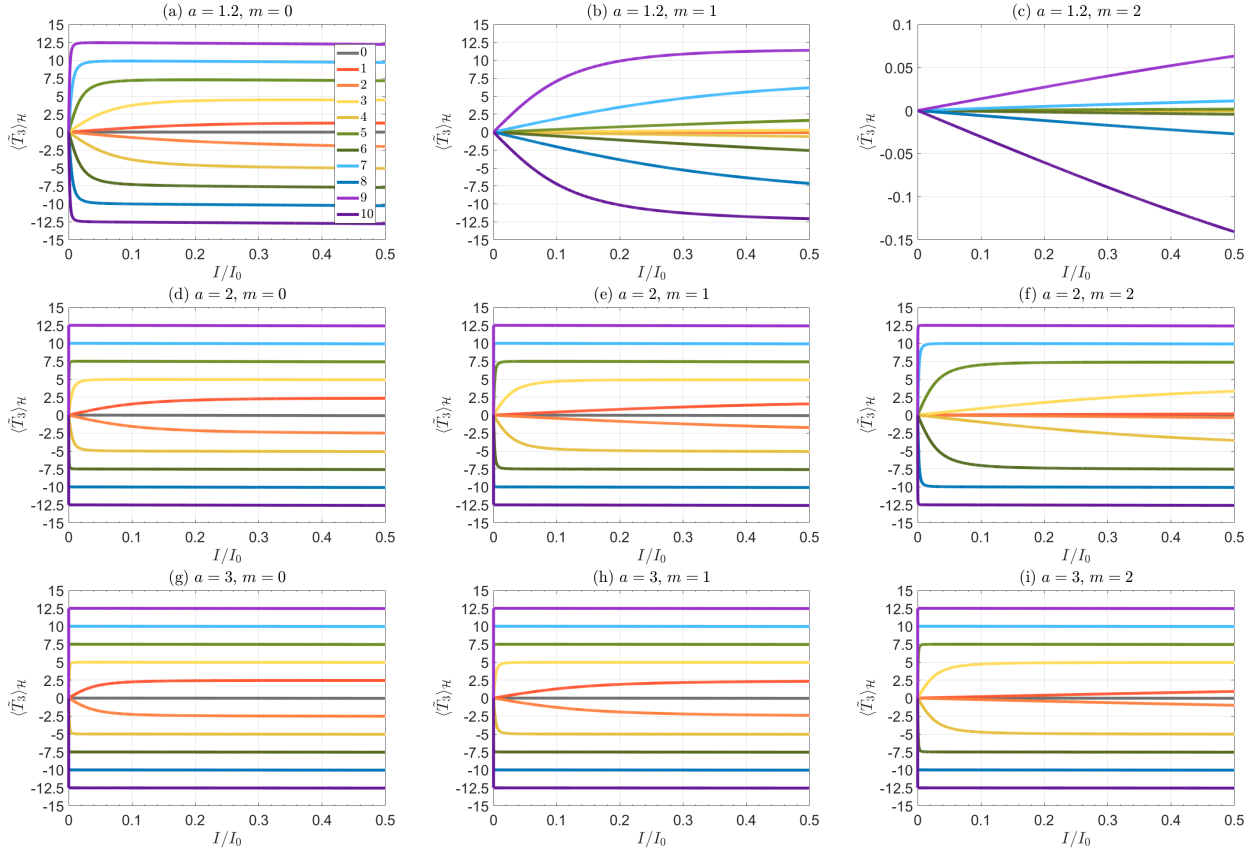


Figure 9: The expectation vales of \hat{T}_3 on the Hamiltonian eigenstates vs. I (in I_0 units) for $a = 1.2, 2, 3$ and $m = 0, 1, 2$, as indicated in each plot. The legend, shown only once, is the same in every plot: 0 = ground state, 1 = first excited state, 2 = second excited state, ...

6 Acknowledgments

The work was financially supported by the projects PN 23210101/2023 and ELI-RO 81-44/2020.

A Analytical expression for $I_n(a)$

We want find analytical expressions for the integrals

$$I_n(a) \equiv \frac{1}{2\pi} \int_0^{2\pi} \frac{e^{in\theta}}{a + \cos\theta} d\theta. \quad (50)$$

For this, we write

$$\frac{1}{2}(I_{n+1} + I_{n-1}) + aI_n = \frac{1}{2\pi} \int_0^{2\pi} \frac{e^{in\theta} \frac{1}{2}(e^{i\theta} + e^{-i\theta}) + e^{in\theta} a}{a + \cos(\theta)} d\theta = \frac{1}{2\pi} \int_0^{2\pi} e^{in\theta} d\theta = \delta_n \quad (51)$$

We obtain two cases: Case i) $n = 0$

$$\frac{1}{2}(I_1(a) + I_{-1}(a)) + aI_0(a) = 1 \quad (52)$$

Case ii) $n \neq 0$

$$\frac{1}{2}(I_{n+1}(a) + I_{n-1}(a)) + aI_n(a) = 0 \quad (53)$$

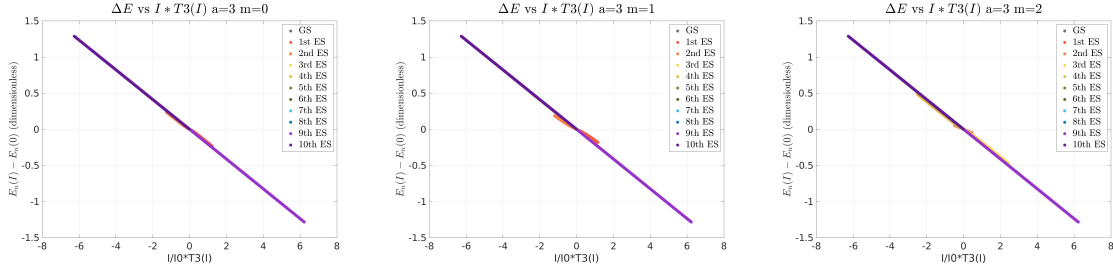


Figure 10: The relation between the energy level splitting and the product $(I/I_0)\langle\tilde{T}_3\rangle_n$, at $a = 3$ and $m = 0, 1, 2$. We see that $\Delta\tilde{E}_n^{(I)} \approx (2/5)(I/I_0)\langle\tilde{T}_3\rangle_n$ and the approximation gets better and better as η increases.

From cases i) and ii) we get a recurrence relation

$$I_{n+1}(a) + 2aI_n(a) + I_{n-1}(a) = 0 \quad (54)$$

which has the characteristic equation for $n > 0$

$$\lambda^2 + 2a\lambda + 1 = 0. \quad (55)$$

From Eq. (55) we obtain

$$I_n(a) = C_1(a) \left(-a - \sqrt{a^2 - 1}\right)^n + C_2(a) \left(-a + \sqrt{a^2 - 1}\right)^n.$$

We need $C_1(a)$ and $C_2(a)$ in order to find a general relation for $I_n(a)$. For this, we make the following observations:

$$-a - \sqrt{a^2 - 1} = \frac{1}{-a + \sqrt{a^2 - 1}} \quad \text{and} \quad I_n = I_n^* = I_{-n}. \quad (56)$$

Then, we have two possibilities:

$$I_n(a) = C(a) \left(-a - \sqrt{a^2 - 1}\right)^n, \quad \text{or} \quad (57a)$$

$$I_n(a) = C(a) \left(-a + \sqrt{a^2 - 1}\right)^n. \quad (57b)$$

Plugging the forms (57) into the condition (52) we get $C(a) = \pm 1/\sqrt{a^2 - 1}$, where the “-” and “+” signs correspond to the possibilities (57a) and (57b), respectively. Since $I_0(a) > 0$, it follows that

$$C(a) = \frac{1}{\sqrt{a^2 - 1}} \quad \text{and} \quad I_n(a) = \frac{(-a + \sqrt{a^2 - 1})^{|n|}}{\sqrt{a^2 - 1}}. \quad (58)$$

B The matrix elements of \hat{T}_3 in the momentum basis

We compute the matrix elements of the z component of the toroidal dipole operator \hat{T}_3 (29). Using the definitions (19) and (29), we obtain

$$\begin{aligned} \hat{T}_3^{(j,0)} &\equiv \frac{i\hbar R}{10m_p} \left[\frac{3a \cos(2\theta) + 4(a^2 + 1) \cos \theta + 5a}{2a} \frac{\partial}{\partial \theta} \right], \\ \hat{T}_3^{(j,I)} &\equiv -\frac{i\hbar R}{10m_p} \left[\frac{3a \cos(2\theta) + 4(a^2 + 1) \cos \theta + 5a}{2a} \frac{iqR}{\hbar a} A_\theta \right], \end{aligned}$$

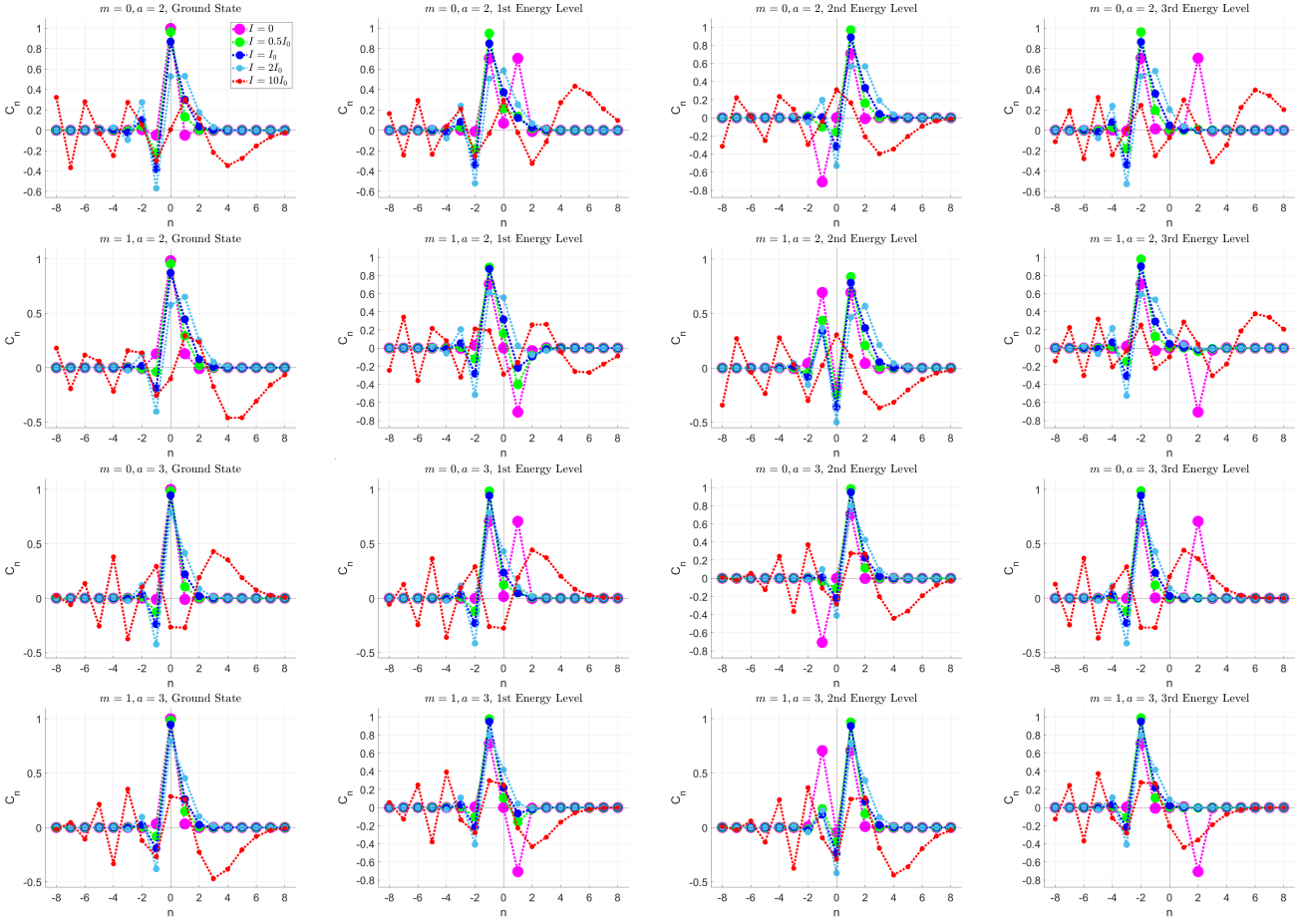


Figure 11: The coefficients of the Hamiltonian eigenstates in the $\{\mathcal{F}_{n,m}^{(\Lambda)}\}$ basis.

$$\langle \mathcal{F}_{n_1, m_1}^{(\Lambda)} | \tilde{T}_3^{(j,0)} | \mathcal{F}_{n_2, m_2}^{(\Lambda)} \rangle \equiv i \delta_{m_1, m_2} [K_1(n_2, n_2 - n_1) + K_2(n_2 - n_1)], \quad \text{where} \quad (59)$$

$$K_1(n_2, n) = \frac{1}{4\pi a} \int_0^{2\pi} d\theta e^{in\theta} \{in_2 [3a \cos(2\theta) + 4(a^2 + 1) \cos \theta + 5a] + (3a \cos \theta - a^2 + 2) \sin \theta\}$$

$$K_2(n) = \frac{a^2 - 1}{4\pi} \int_0^{2\pi} d\theta e^{in\theta} \frac{\sin \theta}{(a + \cos \theta)} d\theta$$

(in the second and third line we used $n \equiv n_2 - n_1$). For K_1 we obtain immediately

$$\begin{aligned} K_1(n_2, n) &= \frac{3i}{4} \left(n_2 - \frac{1}{2}\right) \delta_{n+2,0} + \frac{3i}{4} \left(n_2 + \frac{1}{2}\right) \delta_{n-2,0} + \frac{i}{4a} [4n_2 (a^2 + 1) + a^2 - 2] \delta_{n+1,0} \\ &\quad + \frac{i}{4a} [4n_2 (a^2 + 1) - a^2 + 2] \delta_{n-1,0} + \frac{5in_2}{2} \delta_{n,0}. \end{aligned} \quad (60)$$

For $K_2(n)$, we first observe that it is imaginary and

$$K_2(-n) = K_2^*(n) = -K_2(n). \quad (61)$$

Then, we may write

$$aK_2(n) + \frac{1}{2}[K_2(n-1) + K_2(n+1)] = i \frac{a^2 - 1}{4} (\delta_{n-1,0} - \delta_{n+1,0}).$$

Directly computing

$$K_2(0) = 0, \quad K_2(1) = -i \frac{(a^2 - 1)}{2} \left(\sqrt{a^2 - 1} - a \right), \quad K_2(2) = -i \frac{(a^2 - 1)}{2} \left(\sqrt{a^2 - 1} - a \right)^2, \quad (62)$$

we can check that Eq. (62) is satisfied. Then, for any $n > 1$ we have the recurrence relation

$$a \cdot K_2(n) + \frac{1}{2} [K_2(n-1) + K_2(n+1)] = 0, \quad (63)$$

with the solutions

$$K_2(n) = \begin{cases} C_1 (-a - \sqrt{a^2 - 1})^n & \text{or} \\ C_2 (-a + \sqrt{a^2 - 1})^n. \end{cases} \quad (64)$$

Comparing (64) with (62) we finally obtain

$$K_2(n) = -i \operatorname{sgn}(n) \frac{(a^2 - 1)}{2} \left(\sqrt{a^2 - 1} - a \right)^{|n|}, \quad (65)$$

where we consider that $\operatorname{sgn}(0) = 0$. Plugging Eqs. (60) and (65) into (59) we obtain

$$\begin{aligned} \langle \mathcal{F}_{n_2-n, m_1}^{(\Lambda)} | \tilde{T}_3^{(j,0)} | \mathcal{F}_{n_2, m_2}^{(\Lambda)} \rangle &= -\delta_{m_1, m_2} \left\{ \frac{3}{4} \left[n_2 (\delta_{n+2,0} + \delta_{n-2,0}) - \frac{1}{2} (\delta_{n+2,0} - \delta_{n-2,0}) \right] + n_2 \frac{a^2 + 1}{a} (\delta_{n+1,0} + \delta_{n-1,0}) \right. \\ &\left. + \frac{a^2 - 2}{4a} (\delta_{n+1,0} - \delta_{n-1,0}) + \frac{5n_2}{2} \delta_{n,0} - \operatorname{sgn}(n) \frac{(a^2 - 1)}{2} \left(\sqrt{a^2 - 1} - a \right)^{|n|} \right\} \end{aligned} \quad (66)$$

For the electromagnetic contribution we have

$$\begin{aligned} \langle \mathcal{F}_{n_2-n, m_1}^{(\Lambda)} | \tilde{T}_3^{(j,I)} | \mathcal{F}_{n_2, m_2}^{(\Lambda)} \rangle &= \frac{I}{4a^2 I_0} \delta_{m_1, m_2} \left\{ \log \left(\frac{2aL}{R} \right) \left[\frac{3a}{4} (\delta_{n+3,0} + \delta_{n-3,0}) + (a^2 + 1) (\delta_{n+2,0} + \delta_{n-2,0}) \right] \right. \\ &+ \frac{13a}{4} (\delta_{n+1,0} + \delta_{n-1,0}) + 2(a^2 + 1) \delta_{n,0} \left. - \left[\frac{3a}{4} (I_{n+3}^{(\ln)}(a) + I_{n-3}^{(\ln)}(a)) + (a^2 + 1) (I_{n+2}^{(\ln)}(a) + I_{n-2}^{(\ln)}(a)) \right] \right. \\ &\left. + \frac{13a}{4} (I_{n+1}^{(\ln)}(a) + I_{n-1}^{(\ln)}(a)) + 2(a^2 + 1) I_n^{(\ln)}(a) \right\}, \end{aligned} \quad (67)$$

with the notation

$$I_n^{(\ln)}(a) = \frac{1}{2\pi} \int_0^{2\pi} e^{in\theta} \log(a + \cos \theta) d\theta = \frac{I_{n-1}(a) - I_{n+1}(a)}{n} \Big|_{n \neq 0} - \log \left(\frac{2}{a + \sqrt{a^2 - 1}} \right) \delta_n. \quad (68)$$

C A simple 2D model

The 2D matrix equation

$$\begin{pmatrix} 1 & \epsilon \\ \epsilon & 1 \end{pmatrix} \mathbf{v} = \alpha \mathbf{v}, \quad (69)$$

has two solutions, one symmetric (+) and one antisymmetric (-),

$$\mathbf{v}^{(\pm)} = \frac{1}{\sqrt{2}} \begin{pmatrix} 1 \\ \pm 1 \end{pmatrix} \quad \text{with} \quad \alpha^{(\pm)} = 1 \pm \epsilon. \quad (70)$$

We assume that ϵ is a small and positive variable and we add a perturbation $\pm\delta$ to the diagonal elements of the matrix (including the variables ϵ and δ in the notations of the eigenvalues and eigenvectors),

$$\begin{pmatrix} 1 + \delta & \epsilon \\ \epsilon & 1 - \delta \end{pmatrix} \mathbf{v}(\epsilon, \delta) = \alpha(\epsilon, \delta) \mathbf{v}(\epsilon, \delta). \quad (71)$$

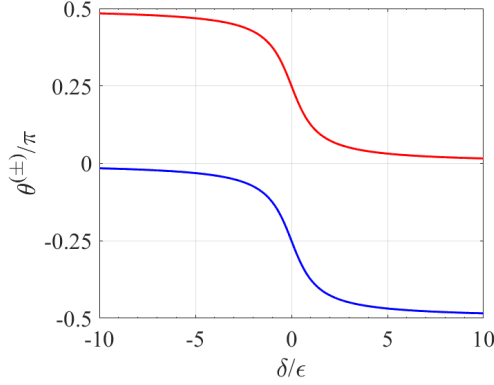


Figure 12: The angles $\theta^{(+)}$ (red line) and $\theta^{(-)}$ (blue line), as functions of δ/ϵ . At $\delta = 0$, $\theta^{(+)}$ corresponds to the symmetric solution, whereas $\theta^{(-)}$ corresponds to the antisymmetric one.

Equation (71) gives the solutions

$$\alpha^{(\pm)}(\epsilon, \delta) = 1 \pm \sqrt{\epsilon^2 + \delta^2}, \quad \mathbf{v}^{(\pm)}(\epsilon, \delta) = N^{(\pm)}(\epsilon, \delta) \begin{pmatrix} 1 \\ -\frac{\delta}{\epsilon} \pm \sqrt{1 + \frac{\delta^2}{\epsilon^2}} \end{pmatrix}, \quad N^{(\pm)}(\epsilon, \delta) = \frac{1}{\sqrt{2\sqrt{1 + \frac{\delta^2}{\epsilon^2}} \left(\sqrt{1 + \frac{\delta^2}{\epsilon^2}} \mp \frac{\delta}{\epsilon} \right)}}. \quad (72)$$

We represent the vectors $\mathbf{v}^{(\pm)}(\epsilon, \delta)$ as complex numbers

$$\zeta^{(\pm)}(\epsilon, \delta) \equiv N^{(\pm)}(\epsilon, \delta) \left[1 + i \left(-\frac{\delta}{\epsilon} \pm \sqrt{1 + \frac{\delta^2}{\epsilon^2}} \right) \right] \equiv e^{i\theta^{(\pm)}(\epsilon, \delta)}, \quad \text{where} \quad \tan \left(\theta^{(\pm)}(\epsilon, \delta) \right) \equiv -\frac{\delta}{\epsilon} \pm \sqrt{1 + \frac{\delta^2}{\epsilon^2}}, \quad (73)$$

and in Fig. 12 we plot the angles $\theta^{(\pm)}(\epsilon, \delta)$. At $\delta = 0$, we recover the symmetric and antisymmetric solutions, $\theta^{(+)}(\epsilon, 0) = \pi/4$ and $\theta^{(-)}(\epsilon, 0) = -\pi/4$, respectively, whereas at $\delta/\epsilon \rightarrow \pm\infty$ we have $\lim_{(\delta/\epsilon) \rightarrow \infty} \theta^{(+)}(\delta, \epsilon) = 0$, $\lim_{(\delta/\epsilon) \rightarrow \infty} \theta^{(-)}(\delta, \epsilon) = -\pi/2$, $\lim_{(\delta/\epsilon) \rightarrow -\infty} \theta^{(+)}(\delta, \epsilon) = \pi/2$, and $\lim_{(\delta/\epsilon) \rightarrow -\infty} \theta^{(-)}(\delta, \epsilon) = 0$.

D Taylor expansions for $I_n(a)$ and $I_n^{(\ln^2)}(a)$

It is useful to calculate the Taylor expansions in the lowest order of $I_n(a)$ and $I_n^{(\ln^2)}(a)$, when $a \gg 1$. For $I_n(a)$ we simply obtain

$$I_n(a) \stackrel{a \gg 1}{\approx} \frac{1}{a} \left(\frac{-1}{2a} \right)^{|n|} \quad (74)$$

The calculation for $I_n^{(\ln^2)}(a)$ is more complicated. First, we write

$$\begin{aligned} I_n^{(\ln^2)} &= \frac{1}{2\pi} \int_0^{2\pi} e^{in\theta} \left[\ln^2 a + \frac{\cos^2 \theta}{a^2} + \frac{\cos^4 \theta}{(2a^2)^2} + \frac{\cos^6 \theta}{(3a^3)^2} + \dots + 2 \ln a \left(\frac{\cos \theta}{a} - \frac{\cos^2 \theta}{2a^2} + \frac{\cos^3 \theta}{3a^3} - \frac{\cos^4 \theta}{4a^4} + \dots \right) \right. \\ &\quad \left. + \sum_{m=3}^{\infty} (-1)^{m-2} \frac{\cos^m \theta}{a^m} \sum_{k=1}^{m-1} \frac{1}{(m-k)k} \right] d\theta \end{aligned} \quad (75)$$

Then, in the lowest order of approximation for each term m , we retain

$$\cos^m \theta = \left(\frac{e^{i\theta} + e^{-i\theta}}{2} \right)^m \approx \frac{e^{im\theta} + e^{-im\theta}}{2} \quad (76)$$

since the other terms give higher orders of approximation. Plugging (76) into (75) and using the identity

$$\sum_{k=1}^{m-1} \frac{m}{k(m-k)} = \sum_{k=1}^{m-1} \left(\frac{1}{k} + \frac{1}{m-k} \right) = 2 \sum_{k=1}^{m-1} \frac{1}{k}$$

we get

$$\begin{aligned} I_n^{(\ln^2)}(a) \stackrel{a \gg 1}{\approx} & \ln^2 a \delta_n + \sum_{m=1}^{\infty} \frac{\delta_{n+2m} + \delta_{n-2m}}{2m^2 a^{2m}} + \ln a \left(\frac{\delta_{n+1} + \delta_{n-1}}{a} - \frac{\delta_{n+2} + \delta_{n-2}}{2a^2} \right) \\ & + \sum_{m=3}^{\infty} (-1)^m \left[\left(\sum_{k=1}^{m-1} \frac{1}{k} \right) - \ln a \right] \frac{\delta_{n+m} + \delta_{n-m}}{ma^m}. \end{aligned} \quad (77)$$

Therefore,

$$I_0^{(\ln^2)} \stackrel{a \gg 1}{\approx} \ln a, \quad I_1^{(\ln^2)} \stackrel{a \gg 1}{\approx} \frac{\ln a}{a}, \quad I_2^{(\ln^2)} \stackrel{a \gg 1}{\approx} -\frac{\ln a}{2a^2} + \frac{1}{2a^2} \quad (78)$$

References

- [1] Ya. B. Zeldovich. Electromagnetic interaction with parity violation. *Sov. Phys.-JETP*, 6:1184, 1958.
- [2] V M Dubovik and A A Cheshkov. Form-factors and multipoles in electromagnetic interactions. *Sov. Phys. JETP*, 24, 1965.
- [3] V M Dubovik and A A Cheshkov. Multipole expansion in classical and quantum field theory and radiation. *Sov. J. Particles Nucl.*, 5:318, 1974.
- [4] S. Nanz. *Toroidal Multipole Moments in Classical Electrodynamics: An Analysis of their Emergence and Physical Significance*. BestMasters. Springer Fachmedien Wiesbaden, 2016.
- [5] Nikitas Papasimakis, V.A. Fedotov, Vassili Savinov, T.A. Raybould, and N.I. Zheludev. Electromagnetic toroidal excitations in matter and free space. *Nature Mat.*, 15:263, 2016.
- [6] V. V. Flambaum. Nuclear anapole moment and tests of the standard model. *AIP Conference Proceedings*, 477(1):14, 1999.
- [7] C. S. Wood, S. C. Bennett, D. Cho, B. P. Masterson, J. L. Roberts, C. E. Tanner, and C. E. Wieman. Measurement of parity nonconservation and an anapole moment in cesium. *Science*, 275(5307):1759, 1997.
- [8] C. M. Ho and R. J. Scherrer. Anapole dark matter. *Phys. Lett. B*, 722:341, 2013.
- [9] Luis G. Cabral-Rosetti, Myriam Mondragón, and Esteban Reyes-Pérez. Anapole moment of the lightest neutralino in the cMSSM. *Nucl. Phys. B*, 907:1, 2016.
- [10] E. E. Radescu. On the electromagnetic properties of majorana fermions. *Phys. Rev. D*, 32:1266, 1985.
- [11] Dubovik Vladimir M. and Valentin E. Kuznetsov. The toroid dipole moment of the neutrino. *International Journal of Modern Physics A*, 13:5257, 1998.
- [12] Charles Kittel. Theory of the structure of ferromagnetic domains in films and small particles. *Phys. Rev.*, 70:965–971, 1946.
- [13] V.M. Dubovik and V.V. Tugushev. Toroid moments in electrodynamics and solid-state physics. *Phys. Rep.*, 187:145, 1990.
- [14] A. Ceulemans, L. F. Chibotaru, and P. W. Fowler. Molecular anapole moments. *Phys. Rev. Lett.*, 80:1861, 1998.
- [15] Daniel Khomskii. Classifying multiferroics: Mechanisms and effects. *Physics*, 2:20, 2009.

- [16] Aleksandr Pyatakov and Anatoly Zvezdin. Magnetolectric and multiferroic media. *Physics-Uspeski*, 55:557, 2012.
- [17] N. Tolstoi and A. Spartakov. Aromagnetism: A new type of magnetism. *J. Exp. Theor. Phys. Lett.*, 52:161, 01 1990.
- [18] V.A. Fedotov, K. Marinov, Allan Boardman, and N.I. Zheludev. On the aromagnetism and anapole moment of anthracene nanocrystals. *New J. Phys.*, 9:95, 04 2007.
- [19] Pierre Tolédano, Dmitry Khalyavin, and Laurent Chapon. Spontaneous toroidal moment and field-induced magnetotoroidic effects in $Ba_2CoGe_2O_7$. *Phys. Rev. B*, 84:094421, 2011.
- [20] Takahiro Shimada, Yuuki Ichiki, Gen Fujimoto, Le Lich, Tao Xu, Jie Wang, and Hiroyuki Hirakata. Ferrotoroidic polarons in antiferrodistortive $SrTiO_3$. *Phys. Rev. B*, 101, 2020.
- [21] Yu Popov, A. Kadomtseva, G. Vorob'ev, VA Timofeeva, D. Ustinin, Anatoly Zvezdin, and M. Tegeranchi. Magnetolectric effect and toroidal ordering in $Ga_{2-x}Fe_xO_3$. *Journal of Experimental and Theoretical Physics*, 87:146, 07 1998.
- [22] Jannis Lehmann, Claire Donnelly, Peter Derlet, Laura Heyderman, and Manfred Fiebig. Poling of an artificial magneto-toroidal crystal. *Nature Nanotechnology*, 14:141, 2019.
- [23] A. Ahmadivand, B. Gerislioglu, and Z. Ramezani. *Toroidal Metamaterials*. Springer, Cham, Springer Nature Switzerland AG.
- [24] I. I. Naumov, L. Bellaiche, and H. Fu. Unusual phase transitions in ferroelectric nanodisks and nanorods. 432:737, 2004.
- [25] K. Marinov, A. D. Boardman, V. A. Fedotov, and N. Zheludev. Toroidal metamaterial. *New J. Phys.*, 9:324, 2007.
- [26] T. Kaelberer, V. A. Fedotov, N. Papasimakis, D. P. Tsai, and Zheludev N. I. Toroidal dipolar response in a metamaterial. *Science*, 330:1510, 2010.
- [27] Alexey A. Basharin, Maria Kafesaki, Eleftherios N. Economou, Costas M. Soukoulis, Vassili A. Fedotov, Vassili Savinov, and Nikolay I. Zheludev. Dielectric metamaterials with toroidal dipolar response. *Phys. Rev. X*, 5:011036, Mar 2015.
- [28] Y. Yang and S. I. Bozhevolnyi. Nonradiating anapole states in nanophotonics: from fundamentals to applications. *Nanotechnology*, 30:204001, 2019.
- [29] V Savinov, N Papasimakis, D P Tsai, and N I Zheludev. Optical anapoles. *Communications Physics*, 2:10, 2019.
- [30] Nahid Talebi, Surong Guo, and Peter Aken. Theory and applications of toroidal moments in electrodynamics: Their emergence, characteristics, and technological relevance. *Nanophotonics*, 7, 1 2017.
- [31] E. Gurvitz, K. Ladutenko, P. Dergachev, A. Evlyukhin, A. Miroschnichenko, and A. Shalin. The high-order toroidal moments and anapole states in all-dielectric photonics. *Laser and Photonics Reviews*, 13:1800266, 2019.
- [32] Alexandre Zagoskin, A. Chipouline, Evgeni Il'ichev, Robert Johansson, and Franco Nori. Toroidal qubits: Naturally-decoupled quiet artificial atoms. *Scientific Reports*, 5, 2014.
- [33] Y. He, G. Guo, T. Feng, Y. Xu, and A. E. Miroschnichenko. Toroidal dipole bound states in the continuum. *Phys. Rev. B*, 98:161112, 2018.
- [34] W. Huang, S. Yin, K. Wang, Y. Zhang, and J. Han. Robust and broadband integrated terahertz coupler conducted with adiabatic following. *New J. Phys.*, 21:113004, 2019.
- [35] Yu Liang, Fengchun Zhang, Xu-Guang Huang, and Huicheng Zheng. Polarization-controlled triple-band absorption in all-metal nanostructures with magnetic dipoles and anapole responses. *Appl. Phys. Express*, 12:062014, 2019.

- [36] N. Pavlov, I. Stenishchev, A. Ospanova, P. Belov, P. Kapitanova, and A. Basharin. Toroidal dipole mode observation in situ. *Physica Status Solidi (b)*, 257:1900406, 2020.
- [37] M. Li, Q. Ma, A. Luo, and W. Hong. Multiple toroidal dipole symmetry-protected bound states in the continuum in all-dielectric metasurfaces. *Optics & Laser Technology*, 154:108252, 2022.
- [38] T. Yezekyan, V. A. Zenin, J. Beermann, and S. I. Bozhevolnyi. Anapole states in gap-surface plasmon resonators. *Nano Lett.*, 22:6098–6104, 2022.
- [39] S. B. Saadatmand, V. Ahmadi, and S. M. Hamidi. Quasi-bic based all-dielectric metasurfaces for ultra-sensitive refractive index and temperature sensing. *Sci. Rep.*, 13:20625, 2023.
- [40] A Costescu and E.E Radescu. Dynamic toroid polarizability of atomic hydrogen. *Ann. Phys.*, 209:13, 1991.
- [41] D. V. Anghel. Mathematical considerations regarding the toroidal momentum operator. *J. Phys. A: Math. Gen.*, 30:3515–3525, 1997.
- [42] D. V. Anghel and A. T. Preda. Quantized toroidal dipole eigenvalues in nano-systems. *J. Phys.: Conf. Ser.*, 2090:012151, 2021.
- [43] M. Dolineanu, A. T. Preda, and D. V. Anghel. The toroidal dipole operator in nanostructures. *Physica A*, 598:127377, 2022.
- [44] D. V. Anghel and M. Dolineanu. The eigenvalues and eigenfunctions of the toroidal dipole operator. *Physica Scripta*, 98:015223, 2022.
- [45] M. Dolineanu, A. T. Preda, and D. V. Anghel. Corrigendum to “the toroidal dipole operator in nanostructures” [physica a 598 (2022) 127377]. *Physica A*, 617:128684, 2023.